

THE PERFORMANCE OF RENEWABLE BICYCLE CHAIN LUBRICANTS

by

Bill Michelsen

A thesis submitted to the Faculty of the University of Delaware in partial fulfillment of the requirements for the degree of Bachelor of Science in Chemical Engineering with Distinction

Spring 2015

© 2015 Bill Michelsen
All Rights Reserved

THE PERFORMANCE OF RENEWABLE BICYCLE CHAIN LUBRICANTS

by

Bill Michelsen

Approved: _____
Mark B. Shiflett, Ph.D., P.E.
Professor in charge of thesis on behalf of the Advisory Committee

Approved: _____
Prasad Dhurjati, Ph.D.
Committee member from the Department of Chemical and Biomolecular
Engineering

Approved: _____
Christopher J. Kloxin, Ph.D.
Committee member from the Board of Senior Thesis Readers

Approved: _____
Michelle Provost-Craig, Ph.D.
Chair of the University Committee on Student and Faculty Honors

ACKNOWLEDGMENTS

I would like to extend my thanks to all the people who guided me along the way and made this thesis possible:

- Dr. Shiflett, for giving me the opportunity to work on this research and setting me up for success at every step of the way.
- Dr. Burris, for his invaluable expertise in tribology and tribometer design.
- Dr. Dhurjati and Dr. Kloxin, for providing their guidance and encouragement, and for participating in my defense.
- Axel Moore, for graciously offering his help in every step of the research process and tribometer design.
- Bill McKechnie, Mengguang Yang, Yuan Wei, Paul LaShier, Will McCormick, Ben Matsuura, and Tyler Slouf for their assistance with measuring some of the data presented in this thesis.
- Lauren Barsky, and everyone at the Undergraduate Research Program for their continuous support, both financial and psychological.

TABLE OF CONTENTS

| | |
|--|----|
| LIST OF TABLES | v |
| LIST OF FIGURES | vi |
| ABSTRACT | ix |
| 1 INTRODUCTION AND THEORETICAL BACKGROUND | 1 |
| 1.1 Problem Statement..... | 1 |
| 1.2 Objectives | 2 |
| 1.3 Literature Review | 4 |
| 1.3.1 The Field of Tribology | 4 |
| 1.3.2 Theoretical Background: Friction..... | 5 |
| 1.3.3 Theoretical Background: Wear..... | 9 |
| 1.3.4 Lubricant Composition and Lubrication Theory | 14 |
| 1.3.5 Bicycle Chain Forces and Power Loss Calculations | 21 |
| 2 EXPERIMENTAL METHODOLOGY AND CONSTRUCTION OF THE TRIBOMETER APPARATUS | 27 |
| 2.1 Experimental Details | 27 |
| 2.2 Tribometer Design..... | 30 |
| 3 FRICTION AND POWER LOSS RESULTS | 44 |
| 4 WEAR RESULTS | 49 |
| 5 LUBRICANT STABILITY AND FUTURE WORK | 54 |
| 5.1 Bio-derived Lubricant Stability | 54 |
| 5.2 Future Work..... | 56 |
| REFERENCES | 58 |
| APPENDIX | 61 |
| A LUBRICANT INFORMATION | 61 |
| B DETAILED TRIBOMETER BLUEPRINTS..... | 63 |
| B.1 Stage, Legs, and Spindle | 63 |
| B.2 Load Arm and Flexure Arms..... | 68 |
| B.3 Back Mounting Plate and Spring Clamps | 70 |
| B.4 Stopper Arms and Ball Bearing Holder..... | 75 |

LIST OF TABLES

| | |
|---|----|
| Table A.1: Commercial lubricant samples with respective abbreviations. | 61 |
| Table A.2: Natural oil samples with respective abbreviations. | 62 |

LIST OF FIGURES

| | |
|--|----|
| Figure 1.1: Illustration of surface asperities and the effect of the normal load on real contact area..... | 7 |
| Figure 1.2: Process of adhesive wear due to material transfer. Two asperities come into contact and an area of adhesion is formed, causing some material from the top surface to be deposited on the bottom surface after the contact is broken..... | 10 |
| Figure 1.3: Abrasive wear mechanisms and examples are shown. Plowing and cutting illustrations are shown for a two-body interaction (a), and a three-body interaction (b). A typical surface marked with various abrasive wear grooves is given at two different magnifications (c)..... | 12 |
| Figure 1.4: An example of a Stribeck Curve. Coefficient of friction and film thickness are plotted as a function of the bearing parameter. Note that the curve is plotted on a log-log scale. Boundary lubrication, mixed lubrication, and hydrodynamic lubrication regimes are also depicted. ... | 18 |
| Figure 1.5: An illustration of the molecular structure of graphite (a) and PTFE (b). Carbon atoms are arranged in planar hexagonal layers. The long lines represent the weaker forces present between each lattice layer. Fluorine atoms are colored green and carbon atoms are in black. | 20 |
| Figure 1.6: Schematic of a chain link assembly. Four major parts are shown: the outer plates, pins, inner plates, and rollers. | 21 |
| Figure 1.7: Example chain and sprocket system. Relevant angles are labeled along with the links subject to the maximum and minimum normal loads..... | 25 |
| Figure 2.1: Schematic of a pin-on-disc tribometer. A normal load is applied to a holder containing a ball bearing that is placed in contact with a rotating sample. | 28 |
| Figure 2.2: A sample wear track is shown. The track under the interferometer before scanning (a). The color coded track after scan. Blue represents valleys and peaks are shown in red (b). Track profile showing a clear width and depth. Area was calculated using these images (c). | 29 |
| Figure 2.3: Three dimensional CAD model of the stage and spindle system (a). Photo of the completed drivetrain system, including the motor, pulleys, and timing belt (b)..... | 32 |

| | |
|---|----|
| Figure 2.4: Adjustable roller stage assembly. From bottom to top: x-axis stage, tilt stage, z-axis stage. | 33 |
| Figure 2.5: Side and top views of the load arm and spring system. Major components and flexures are labeled accordingly..... | 36 |
| Figure 2.6: Close up photo of the finalized arm and spring system. | 37 |
| Figure 2.7: Final ball bearing holder design. Masses for applying normal load are placed around the rod at the end of the load arm. | 38 |
| Figure 2.8: LVDT alignment and calibration method. The shell mounts to the side flexure arm while the core attaches to a target on the load arm via a nut and washer (a). Various masses are tied to the load arm and hung over a smooth cylinder with fishing line to exert a lateral force, allowing the output voltage to be calibrated to the friction force (b)..... | 41 |
| Figure 2.9: Calibration curves to convert LVDT output voltage to the friction force for spring thicknesses of 0.006" (a) and 0.010" (b). Calibration constants are taken as the best fit slopes of 18.78 mN/V and 88.05 mN/V, respectively..... | 42 |
| Figure 2.10: Profile and front views of the completed tribometer after troubleshooting and optimization. | 43 |
| Figure 3.1: Selected lubricant COF values over a range of linear speeds. Error bars equal to the standard deviation for each lubricant are shown. | 44 |
| Figure 3.2: Coefficient of friction results and corresponding power loss values for common bicycle chain lubricants. | 46 |
| Figure 3.3: Coefficient of friction values for various natural oils..... | 48 |
| Figure 4.1: Wear results for common bicycle chain lubricants..... | 49 |
| Figure 4.2: Effect of anti-wear additive (Lubrizol LZ4370LG) on canola oil base lubricant. Lubricant 1B (Slick Lube 100) is shown as a reference. | 51 |
| Figure 4.3: Plot of wear versus coefficient of friction for various lubricants. | 52 |
| Figure B.1: Mounting stage specifications. | 63 |
| Figure B.2: Stage leg specifications. Four identical legs were machined. | 64 |
| Figure B.3: Stage leg brackets. One attaches the side of each leg to the stage. | 65 |

| | |
|---|----|
| Figure B.4: Spindle housing. Angular contact bearings are fit into the wide spaces cleared at the top and bottom of the cylinder. | 66 |
| Figure B.5: Spindle and sample disc specifications, made from stainless steel. | 67 |
| Figure B.6: Load arm specifications. | 68 |
| Figure B.7: Flexure arm specifications. Two identical arms are needed. | 69 |
| Figure B.8: Back plate. Includes holes for mounting to z-stage and for flexure arm and stopper arm attachments. | 70 |
| Figure B.9: Friction spring clamps. One of these attaches to each end of the load arm. | 71 |
| Figure B.10: Friction spring clamps. One of these attaches to each flexure arm end. . | 72 |
| Figure B.11: Normal spring clamps. Four identical parts are needed: two for each flexure arm and two for each bracket attachment to the back plate. | 73 |
| Figure B.12: Normal spring base brackets. These attach to the back plate and serve as the bases for the two normal force springs. | 74 |
| Figure B.13: Stopper arms to prevent over extension of normal force springs. One is needed for each flexure arm, however one side must have a section cut away to accommodate the friction sensor. | 75 |
| Figure B.14: Ball bearing holder. The inside is threaded for each removal to access to ball for cleaning or replacement. | 76 |

ABSTRACT

Natural or biobased lubricants are desirable on the market today due to their performance as a safe, ecological, and effective product. In this study we report on the friction and wear properties of commercial bicycle lubricants, natural base oils (e.g. canola, soy, etc.), and the effect of certain additives on these properties. A pin-on-disc tribometer was designed and assembled specifically for this study to measure the coefficient of friction and wear on a steel-on-steel contact for each lubricant sample. The design process and finalized schematics of the device are detailed. A correlation was also derived to relate the coefficient of friction of each lubricant to an associated power loss in a bicycle drivetrain. The commercial lubricants had a wide range of friction performance, with Slick Lube 100 giving the lowest COF of 0.042 ± 0.001 (power loss 7.80 ± 0.26 watts), and GT85 having the highest COF of 0.131 ± 0.003 (power loss 24.16 ± 0.51 watts). Wear tests resulted in a large disparity between the best and worst lubricants as well, with three samples effectively rejecting all wear during a one hour test, while the worst performer resulted in a wear track cross sectional area of $15.9 \pm 3.3 \mu\text{m}^2$. The natural oils tested were excellent at reducing friction with an average COF of 0.040 ± 0.004 , although the average wear performance of these oils proved to be worse than the commercial lubricants with an average area loss of $7.45 \pm 1.7 \mu\text{m}^2$. However, it is shown that adding 5% or more by weight of an anti-wear additive can greatly improve this performance. Combining these results we explore possible correlations between friction, wear, viscosity, density, and individual lubricant components or additives.

Chapter 1

INTRODUCTION AND THEORETICAL BACKGROUND

1.1 Problem Statement

Lubrication is perhaps the most important factor in reducing the friction and wear associated with moving parts in any mechanical application. Choosing the right lubricant can be the difference between a successful, efficient design and a complete failure, and therefore should be a major consideration when engineering any type of mechanical application. In the application of bicycle chains, lubrication reduces the wear of the drivetrain components and decreases the amount of force required by the rider to pedal. This makes chain lubrication an important consideration for competitive cyclists and casual riders alike, as choosing an efficient lubricant can shave time off travel and extend the lifetime of a bicycle's drivetrain. Many lubricants today are non-biodegradable and not recommended for contact with the skin. Due to the exposed chain on a bicycle, skin contact is inevitable so a safe and effective lubricant is required. As a chemical engineer, this poses a design problem to create a safe lubricant with high performance. Biodegradable or renewable lubricants have the dual benefit of being safe to handle as well as better for the environment, because their base is typically an oil capable of being broken down through natural processes. Although there is a demand for these kinds of lubricants, not many options exist on the market today. The goal of this research is to determine a composition for a bicycle chain lubricant with optimal friction and wear performance using lubricants that are safe and biodegradable.

1.2 Objectives

Benchmarks for the performance of commercially available bicycle chain lubricants are needed to enable the design of improved renewable lubricants. The first series of experiments were carried out to measure the friction and wear properties of cycling lubricants currently on the market. A selection of about thirty popular lubricants was tested to determine their coefficient of friction (COF) and rate of wear. This information was used to determine a performance standard to compare with the results obtained from various experimental lubricants.

In order to make these results more relatable in the context of cycling, a relation was derived to determine the power loss associated with each lubricant based on their respective coefficients of friction. These calculations were derived from the forces and dimensions involved when the chain moves around the sprocket during pedaling. This power loss corresponds to the efficiency of the lubricant-drivetrain system. Assuming two identical cyclists expending equal amounts of energy, the difference in power loss associated with different lubes will result in different speeds of the two riders. This information will be particularly useful for competitive cyclists, as choosing an efficient lubricant can translate to a measurable improvement in rider performance.

The wear associated with each lubricant is difficult to measure and is therefore rarely reported. This study provides information on the wear rate of different lubricants, which is useful and convenient for any cyclist wishing to prolong the lifetime of their drivetrain components. An effective lubricant will protect the contacting surfaces for an extended time, which results in fewer reapplications necessary to maintain the desired level of lubrication. Results from wear tests can be

used in conjunction with friction data in order to determine the overall performance for each lubricant, which includes both its efficiency and longevity.

After obtaining data for existing lubricants on the market, the next objective is to test individual lubricant components to determine what compounds or mixtures provide optimal friction and wear performance. Numerous natural oils were tested to determine their efficacy as a lubricant, including commonly available products such as canola, soybean, and castor oil. Creating mixtures of different components, combining both natural and synthetic bases, and adding small amounts of additives to a sample yields different results. The overall objective of this study is to determine a lubricant composition that exhibits optimal performance based on the results from these experiments.

1.3 Literature Review

Before beginning any kind of experimentation, it is important to first research and understand the fundamental principles that govern the behavior of the system in question. The experiments in this study fall under the field of tribology, which aims to investigate and quantify the surface interactions that give rise to what we know as friction and wear. This section will outline the basic principles needed to understand and interpret the results outlined in this paper.

1.3.1 The Field of Tribology

When measuring the performance of a lubricant two properties are typically reported: the coefficient of friction and the rate of wear. Both of these properties can be measured quantitatively and precisely using the concepts of tribology. Tribology is defined as the study of the design, friction, wear, and lubrication of interacting surfaces in relative motion, and is generally considered a combination of many different disciplines including chemistry, physics, materials science, and mechanical engineering.²⁵ This field has been consistently growing in importance and popularity since the Jost Report in 1966, which estimated that an enormous amount of resources could be saved from a better understanding of mechanical surface interactions, estimated at about \$900 million per year in the United Kingdom alone.²¹ This report is considered the birth of the modern tribology, as it successfully persuaded the British government to launch a program of education and research to remedy the situation. The most recent estimates put the annual costs of improper lubrication in the hundreds of billions of dollars.¹⁰ It is for this reason that tribology seeks to study and describe friction and wear at a fundamental level, which provides valuable insight for designing new lubricants that will optimize performance and lower costs. The kinds of

experiments carried out in this research are common to the field of tribology, however in the application of bicycle chains and the efficacy of natural oils for lubrication, this research is novel and unique

1.3.2 Theoretical Background: Friction

Friction is defined as the force of resistance that occurs when one body moves tangentially over another body. The first documented scientific study of friction dates back to the 15th century when Leonardo da Vinci first recorded two laws of friction in his notes.¹⁸ Unfortunately, da Vinci's findings were forgotten until 1699 when a French physicist, Guillaume Amontons, rediscovered these laws. Amontons observed that the frictional force F_F is directly proportional to the applied normal force F_N .¹⁸ The parameter of proportionality, commonly denoted by μ , is called the coefficient of friction. Furthermore, Amontons recognized that this coefficient of friction is independent of the contact area of the sliding surfaces. This observation may seem counterintuitive, as it means two blocks with the same mass but different surface areas will experience the same frictional force! Almost a century later, Charles-Augustin de Coulomb, another French physicist, further developed these laws by discovering that the friction force is also independent of the relative velocity of the bodies once the sliding movement begins.¹⁸ These three laws can be summarized by the equation:

$$\mu = \frac{F_F}{F_N} = \text{Constant} \quad (1.1)$$

Equation 1.1 states that the coefficient of friction, μ , is constant and equal to the ratio of friction force and normal force exerted on an object. These early investigators explained this phenomenon by hypothesizing that friction is due to the interlocking of protuberances or asperities on the surfaces of the contacting materials. This explanation

is often referred to as the “roughness hypothesis” and remained the popular view of the scientific community until the early 20th century, when scientists such as Hardy and Tomlinson began to hypothesize that the force of friction is due to adhesion between the surfaces rather than roughness.²¹ This hypothesis, however, was in contradiction to the observation that friction is independent of the area of contact. It was not until 1940 when a number of researchers using a microscopic analysis of friction, namely Holm, Ernst and Merchant, and Bowden and Tabor cleared up this inconsistency by stating that there is a crucial difference between the apparent contact area and the real area of contact, which alone determines the magnitude of the friction force. It was shown that these real areas of contact were proportional to the normal load, but independent of the apparent area, explaining the experimental observations and giving credence to the adhesion hypothesis.

On the microscopic scale it can be seen that surfaces are typically rough and uneven, leading to only a few areas of contact, or asperity points. These points often cover only a small portion of the apparent surface area. When two surfaces are subjected to a compressive load, the real contact area is small, causing the stress over the contacting asperities to be high enough to allow for plastic deformation to occur at these points.² This deformation increases the contact area between the surfaces until it is sufficient to support the load. Figure 1.1 illustrates this phenomenon by showing the effect of the normal load on the true contact area.

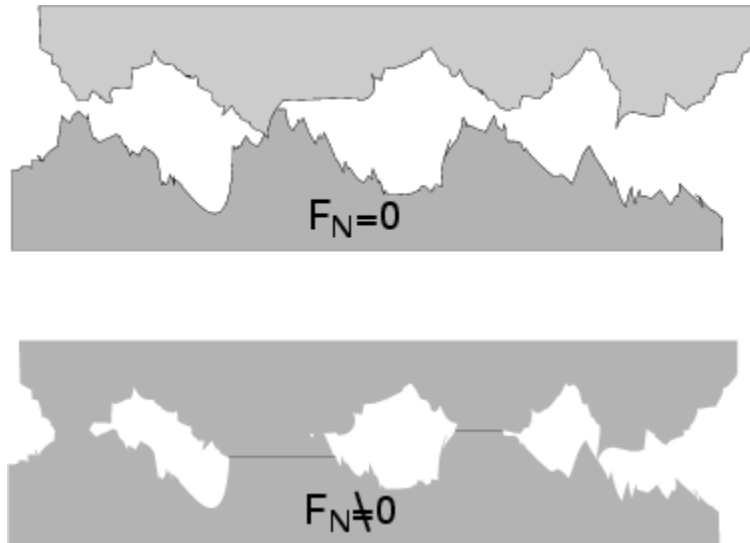


Figure 1.1: Illustration of surface asperities and the effect of the normal load on real contact area.

The contact at the junctions causes a strong adhesion force between atoms of the contacting surfaces. In fact, extremely rough surfaces often display lower friction than that of extremely smooth surfaces, due to the adhesion forces being greater than that of the forces required to lift one surface over the “humps” in the other.²¹ It is known that atom-to-atom forces only occur at extremely small distances, usually just a few angstroms in length. Other interactions do occur at greater distances, but these have been shown to be insignificant to those produced at the junctions that compose the real area of contact.²¹ The main resistance to sliding arises from the need to shear these strongly adherent surface atoms. Using this assumption an equation for the total friction force can be derived.

$$F = A_r \cdot S \quad (1.2)$$

Equation 1.2 states that the total friction force is equal to the product of the real area of contact, A_r , and the force per unit area required to shear the junctions S . It is for

this reason friction is related to material properties as well as the applied load. It is a common assumption that the real area of contact is approximately equal to the applied load L divided by the maximum compressive stress that the material can handle before plastic deformation occurs (hardness), denoted by P .

$$A_r = \frac{L}{P} \quad (1.3)$$

Combining Equations 1.2 and 1.3 another relation for the coefficient of friction can be made.

$$\frac{F}{L} = \mu = \frac{S}{P} \quad (1.4)$$

Equation 1.4 states that the coefficient of friction between two materials is equal to the ratio of the shear strength to the hardness of the weaker material.² This correlation is based on assumptions that are not always correct and therefore the coefficients of friction calculated using this method are often inaccurate compared to those measured experimentally.²¹ However, the basic ideas outlined by the Adhesion Theory of Friction are widely accepted and neatly explain the observed laws of friction. This shows that the COF is difficult, if not impossible, to predict accurately even given all the necessary information about a system.

According to this most recent theory, the majority of the energy loss associated with friction is due to two interactions: adhesion and material displacement. The work lost to friction arises from the need to shear areas of adhesion, in addition to material displacement such as asperity interlocking and plastic deformation. These small scale interactions are not only responsible for friction, but also cause what is commonly known as wear.

1.3.3 Theoretical Background: Wear

Wear, for tribological purposes, is generally defined as the removal of material from solid surfaces as a result of mechanical action.²¹ Although wear is one of the main reasons that items lose their usefulness over time, there is a widespread lack of interest and appreciation of the importance of the subject. This is evidenced by the limited body of published work describing wear, its mechanisms, and its impact. The lack of interest in the subject can be attributed to a number of factors. First, the study of wear has only been approached relatively recently and therefore our knowledge of its laws and behavior is still largely incomplete. Second, wear rates are often quite low and are difficult to measure without the advent of modern techniques and equipment that can be expensive and not widely available. Moreover, wear experiments often show very large variation or error in results, leading to ambiguous conclusions. Lastly, there was a common attitude among many engineers and scientists who believed wear is a phenomenon so complicated and erratic that systematic investigation was bound to be a waste of time.²¹ Therefore, the prevailing course of action was to rely on previous experience and a few simple life tests when designing a new device. As you might imagine, this attitude is still held by the majority of design engineers today. However, this line of thinking can be exceedingly dangerous when completely new situations arise, for example, the sliding motion of mechanisms that will operate in outer space. It is for this reason that a comprehensive understanding of wear is extremely important and is still being investigated today.

Current literature generally has wear broken down into four main categories: adhesive wear, abrasive wear, corrosive wear, and fatigue wear.²⁴ Each process obeys its own laws; however, to confuse matters, one mode of wear will often act in such a way to affect the others. Wear, like friction, occurs at the areas of real contact between

surfaces. Adhesive wear occurs when two surfaces are placed in contact and fragments of one surface are pulled off and adhere to the other. These fragments may then later be transferred back to the original surface, or form loose wear particles. Figure 1.2 provides an illustration of this effect.

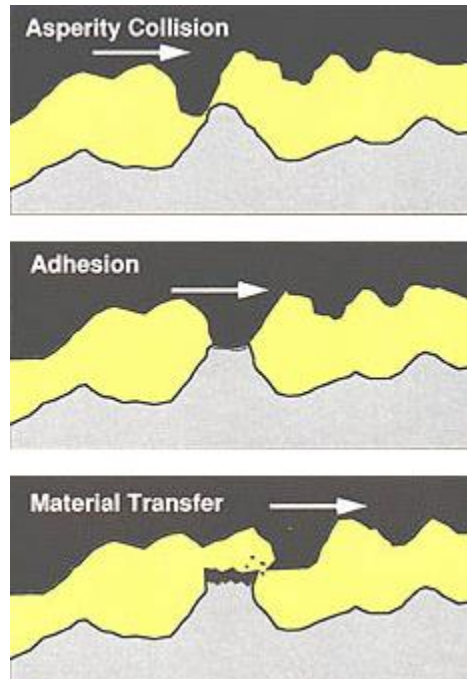


Figure 1.2: Process of adhesive wear due to material transfer. Two asperities come into contact and an area of adhesion is formed, causing some material from the top surface to be deposited on the bottom surface after the contact is broken.

This type of wear is generally miniscule when dealing with metals because of the presence of oxide film on almost all metal surfaces exposed to atmospheric conditions. This film is often only a few nanometers thick, which is still significant enough to prevent true contact between the metals and hinder adhesion.²⁴

Abrasive wear occurs when a material rubs against another object of equal or greater hardness. This can occur when an asperity on the harder surface breaks off a piece of the softer material, or by a three-body interaction, in which the wear is caused by a particle of hard material, or grit, embedded between the two surfaces. In this mode of wear, material may be removed by cutting, plowing, or fracturing the soft surface by the hard surface or grit.²⁸ Cutting occurs when a chip forms in front of the cutting asperity or grit. This material is lost from the surface and the volume lost is equal to the volume of the wear track, or groove, left behind. Plowing is a similar process to cutting, except the material is shifted to the sides of the groove and is not removed from the surface. Fracture occurs when the material cracks in the subsurface regions surrounding the wear groove. Abrasive wear is the most prevalent type of wear in bicycle chains and is therefore used for the measurements taken for this study.

Polishing is actually a specially controlled form of abrasive wear, where the grit is small enough to continuously remove a thin film off of the surface until it is sufficiently smooth. The smoothness of highly polished surfaces is what makes objects shine with a mirror-like finish. A diagram of the mechanisms of abrasive wear is included in Figure 1.3 along with a typical example of an abrasive wear pattern under a microscope.

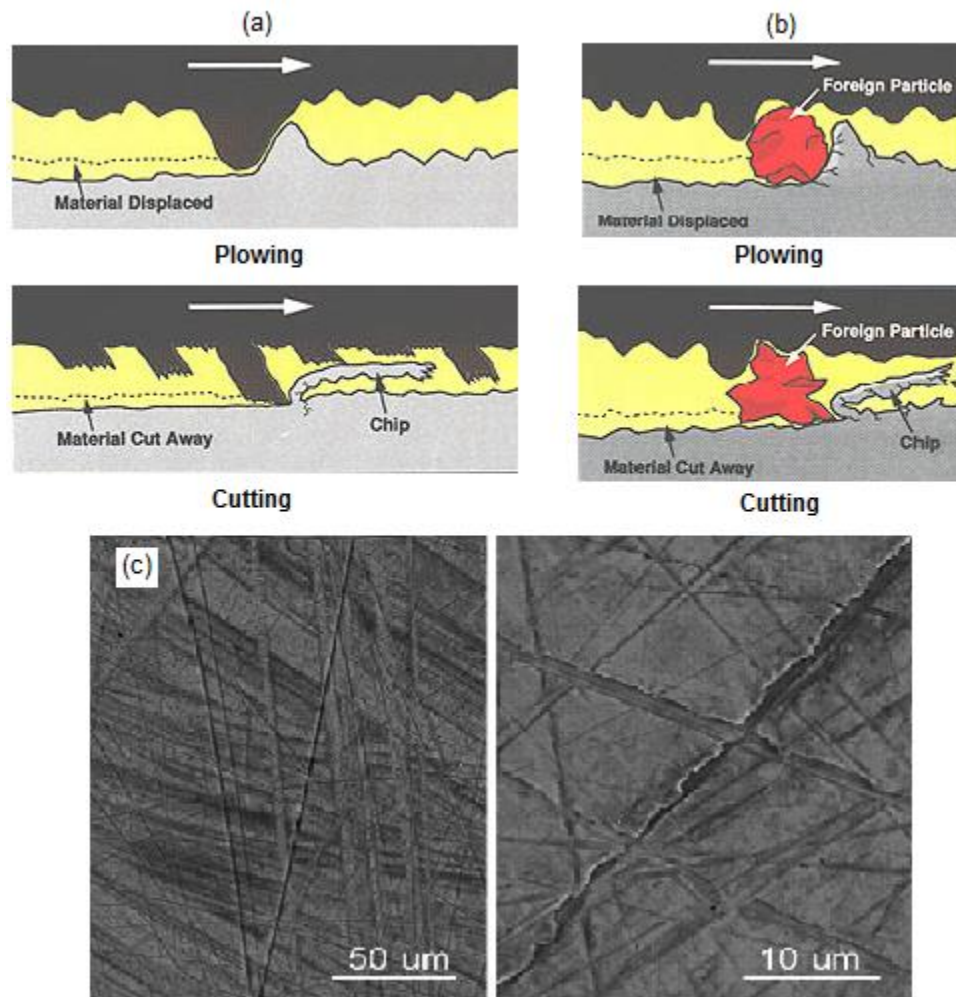


Figure 1.3: Abrasive wear mechanisms and examples are shown. Plowing and cutting illustrations are shown for a two-body interaction (a), and a three-body interaction (b). A typical surface marked with various abrasive wear grooves is given at two different magnifications (c).

Wear may also be caused by the corrosion of the rubbing surfaces. Increased temperature along with the removal of the protective oxide film from the surface due to friction promotes an accelerated oxidation process. The continuous removal of the oxide film along the surface allows for new oxidation to occur, allowing for corrosion

to reach deeper into the material. Hard oxide particle removed from the surface can also become trapped, additionally increasing the rate of wear by the three-body abrasive wear mechanism.¹⁵

The final major category of wear is fatigue wear. This type of wear is produced by repeated rolling or sliding over a track. This continuous motion leads to alternating loading and unloading cycles on the material, which can result in the formation of surface or subsurface cracks. Cracks will eventually form even if the stress reversals are within the elastic range limits of the material. Once formed, these cracks can then propagate and connect, causing large fragments to form and separate from the surface entirely. Fatigue wear can result in more severe and easily visible damage than the other types of wear discussed, as large fragments can break off, leaving a noticeable pit in its place.²⁸

Wear can be measured quantitatively by measuring the volume of material lost after a given experiment. It has been found that the amount of wear is generally directly proportional to the load and sliding distance, and inversely proportional to the hardness of the surface being worn away. A simple relation has been developed as a result of these experiments in the case of adhesive and abrasive wear, given by

$$V = \frac{kLx}{P} \quad (1.5)$$

Equation 1.5 relates the volume of wear particles generated V to the sliding length x , wear constant k , load L , and hardness of the softer material P .²¹ The wear constant is a non-dimensional value that is dependent on the materials in contact and their degree of cleanliness. The value of k varies over multiple degrees of magnitude, and is generally higher in the case of abrasive wear compared to adhesive wear.²⁸ Evidence for the

validity of Equation 1.5 is mixed, but in almost all cases it represents the experimental data reasonably well.²¹

1.3.4 Lubricant Composition and Lubrication Theory

Lubrication aims to dampen or reduce the interactions that lead to friction and wear, thereby decreasing the required energy input and extending the lifetime of the machinery. Just adding a small amount of lubricant to a process can drastically change its behavior and performance. For example, typical COF values for metal-on-metal sliding can range from 0.4-0.8 for an unlubricated system to below 0.1 for a system with excellent lubrication.²¹ This means the effect of friction can be reduced by over 90% just by adding some lubricant! Lubricants come in many forms and can be comprised of a multitude of different materials. Manufacturers are generally circumspect about the formulation of their products. So what does a lubricant really consist of? The answer almost always includes an oil or a grease.

Oils can be of three origins: biological, mineral, or synthetic, each of which covers a vast array of hydrocarbon compounds. Typical lubricating oils are composed of 95% base stock and 5% additives.²⁴ The physical properties of a lubricant depend on its base, but can also be radically affected by the additives used. Oils from different sources are suited to handle different applications. For example, biological oils are suitable where the risk of contamination must be reduced to a minimum, as in the food or pharmaceutical industries. Biological oils can come from two sources: vegetable or animal. Examples of vegetable oils include castor, palm, and rape-seed oils, while animal based oils include sperm, fish, and wool oils from sheep (lanolin).²⁴ Mineral oils are the most commonly used lubricants throughout industry. They are petroleum based and are typically used in applications where temperature requirements are

moderate. Examples of their areas of application include gears, bearings, engines, and turbines. Synthetic oils are artificially developed substitutes for mineral oils. They are specifically designed to exhibit properties superior to mineral oils for situations that require a more robust lubricant, for example extremely high or extremely low temperature applications.²⁴

Greases are not fundamentally different from oils. They consist of base oil that is mixed with a thickener and other additives to form a solid or semi-solid. The thickener is dispersed within the lubricating oil, producing a stable colloidal structure that constrains the oil and prevents it from flowing freely. Because of this containment of the oil, greases can provide semi-permanent lubrication, and are widely used despite certain limitations in performance.²⁴ Greases must meet the same requirements as oils with the added condition that they must remain semi-solid; if the grease liquefies it will flow away from the contact and the likelihood of failure greatly increases. Additionally, greases are unable to remove heat by convection as oil does, so they are not effective as a cooling agent. Due to these constraints, greases are generally applied in low-maintenance applications such as bearings and gears that do not require a circulating lubrication system for cooling. The lubricating performance of greases is inferior to oils, except in some low sliding speed situations.²⁴

Greases are generally comprised of anywhere between 3-30% thickener and 70-95% oil, with the remainder being additives.²⁶ The nature of the thickener influences the properties of the grease, including its temperature resistance, water resistance, and chemical stability. The most commonly used thickeners are soaps such as lithium, calcium, aluminum, and sodium fatty acid derivatives.²⁶ These form reverse micelle-like complexes resulting in a fibrous structure capable of capturing the

base oil.²⁴ Other thickener options exist, such as silica and bentonite clays, which consist of very fine, porous powders capable of absorbing considerable amounts of oil. When these powders are suspended evenly in the base oil, the resulting grease effectively has no melting point, making them ideal for high temperature applications. These greases are only limited by the oxidation stability of the base oil, which can be improved using various inhibitors.²⁴

Various additives and fillers can also be added to oils and greases to produce desired properties such as anti-oxidants, rust and corrosion inhibitors, extreme pressure additives, and additives that reduce friction and wear. For the application of bicycle chain lubrication, we are mostly interested in the latter. These additives are typically solids that can be suspended in the lubricant matrix. Examples of these materials will be discussed later in this section. In order to understand how the complex mixtures found in most lubricants achieve the observed performance standards, we must closely examine what is happening on a microscopic scale when a lubricant is placed between two sliding surfaces.

Lubrication can be broken down into two different categories: fluid lubrication, where a film of liquid or gas is interposed between the two solid bodies, and solid film lubrication, in which a solid layer of foreign material separates the surfaces. Fluid lubrication is further divided into three main regimes which depend on the lubricant viscosity, load, and speed of the given system. Boundary lubrication refers to the case where the two surfaces are not completely separated by the lubricant film, so some solid contact remains. Hydrodynamic lubrication describes the opposite case, where the lubricant film is thick enough to separate the surfaces entirely. Mixed lubrication occurs in the transition phase between these two regimes.

A useful method of visualizing these phenomena is to compare the film thickness to the surface roughness. If the film thickness is less than the roughness, the lubricant effectively only fills in the cracks between asperities, leading to boundary lubrication. If the two properties are approximately equal, the lubrication is in the mixed regime, and if the film thickness is greater than the roughness, hydrodynamic lubrication occurs. The coefficient of friction and rate of wear will change drastically depending on what lubrication regime the system is in. This relationship is commonly depicted in the form of a Stribeck curve (named after the German engineer Richard Stribeck), where the COF is plotted against a dimensionless bearing parameter. The bearing parameter is often written as $\eta N/P$, where η is the dynamic viscosity of the lubricant, N is the speed (e.g. revolutions per minute of a bearing), and P is the applied load.¹⁴ The shape of this curve is conserved for almost all systems under fluid lubrication. Figure 1.4 provides an example of the Stribeck curve along with illustrations of what is happening in each lubricant regime.

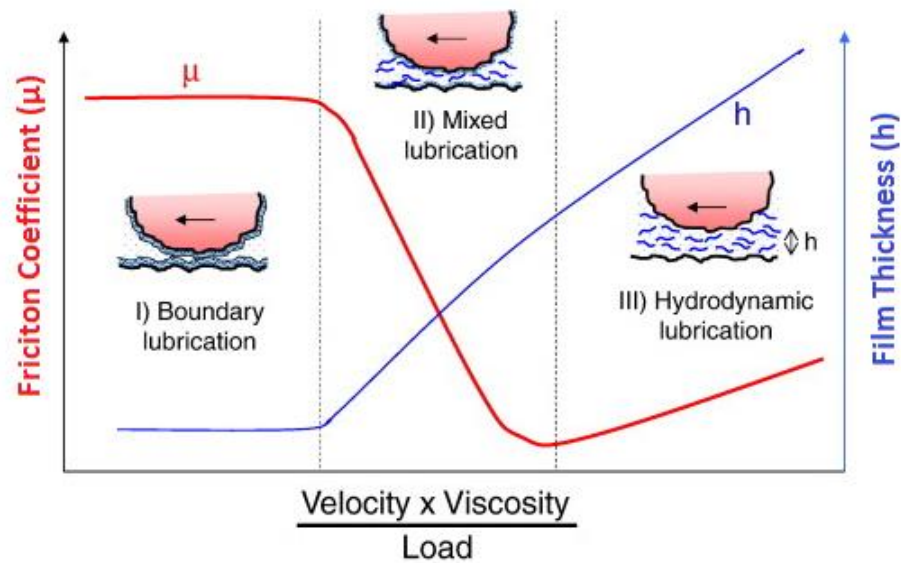


Figure 1.4: An example of a Stribeck Curve. Coefficient of friction and film thickness are plotted as a function of the bearing parameter. Note that the curve is plotted on a log-log scale. Boundary lubrication, mixed lubrication, and hydrodynamic lubrication regimes are also depicted.

Boundary lubrication is undesired as it results in the maximum amount of friction and wear due to the constant contact between surface asperities. In the mixed lubrication regime, a film begins to form and supports some of the load, resulting in the surfaces beginning to separate. The COF declines rapidly during this process due to the surface contact only occurring intermittently, until it reaches a minimum value. Here the system enters the hydrodynamic regime, which is characterized by low friction and little to no wear, since the load is entirely supported by the fluid film. The COF will actually begin to slowly increase in this regime, due to fluid drag increasing at higher speeds and viscosities.¹ A relatable example of this effect is the difficulty of walking in water versus running in water in the case of increased speed, or walking in air versus walking in water in the case of increased viscosity. Viscosity

is an important consideration for bicycle chain lubricants, as a more viscous lubricant generally provides better protection against friction and wear. However if the viscosity is too high it may only coat the outside of the bicycle chain, missing the internal components.¹¹

Oil based lubricants only function properly under conditions that allow for the formation of a fluid film between surfaces. In applications with speeds, temperatures, or pressures outside of this range, solid based lubrication may be the only option. These materials may be applied in the form of an additive to a fluid lubricant, in pure form, or even alloyed into the component surface during manufacturing. Some commonly used solid or dry film lubricants include polytetrafluoroethylene (PTFE), graphite, molybdenum disulfide (MoS_2), boron nitride (BN), talc, and metal oxides.¹³ Crystalline lattice structured materials, such as graphite and molybdenum disulfide powders, are arranged in layers that are individually resistant to penetration but will easily slide past each other. It is these lattice layers with low resistance to shear that minimize the friction between sliding surfaces; it has been thought to be comparable to walking across a room full of flat, slippery plates. An example of this structure in graphite is included in Figure 1.5. These materials are often used in high temperature applications, due to their ability to resist oxidation at extreme temperatures greater than $400\text{ }^\circ\text{C}$ for MoS_2 and $700\text{ }^\circ\text{C}$ for graphite.¹³

The linear long chain polymer PTFE was accidentally discovered by Roy Plunkett, a researcher at DuPont in 1938.¹³ PTFE is inert to virtually all chemicals, does not absorb water, and is considered one of the most slippery materials in existence. It can also be combined with various fillers (e.g. glass fiber, carbon fiber, graphite, and molybdenum disulfide) to enhance certain characteristics such as high

wear resistance, low friction, high creep resistance, and heat dissipation.¹³ The properties of PTFE arise from the aggregate effect of repeated carbon-fluorine bonds. The carbon-fluorine bond is the single strongest bond in organic chemistry and is strengthened even further in the presence of other identical bonds.¹⁷ Since fluorine is highly electronegative and significantly larger than hydrogen, the atoms form an unreactive, slippery armor around the carbon backbone, giving PTFE its extraordinary properties. A representation of this structure is shown in Figure 1.5.

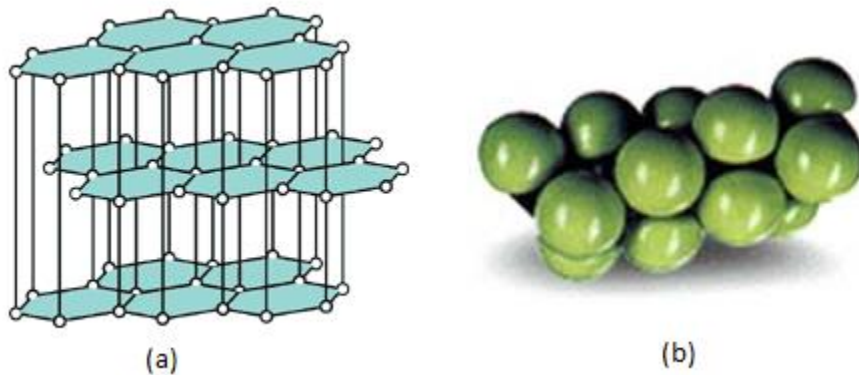


Figure 1.5: An illustration of the molecular structure of graphite (a) and PTFE (b). Carbon atoms are arranged in planar hexagonal layers. The long lines represent the weaker forces present between each lattice layer. Fluorine atoms are colored green and carbon atoms are in black.

Now that the basic details and phenomena behind friction, wear, and lubrication have been outlined, this knowledge must be applied to our goal of creating a superior bicycle chain lubricant. The next section discusses the assembly and forces involved with a bicycle drivetrain and the corresponding power loss due to friction.

1.3.5 Bicycle Chain Forces and Power Loss Calculations

To understand the effects of load, friction, and wear on a bicycle chain it is helpful to begin by examining the basic components of a typical chain assembly. Bicycle chains are classified as roller chains, which consist of two alternating links that when put together create a chain segment. The outer link consists of two outer link plates connected by two pressed-in cross pins, while the inner link consists of two inner plates and two slip-fit rollers. An image containing these parts and how they are assembled is shown in Figure 1.6.

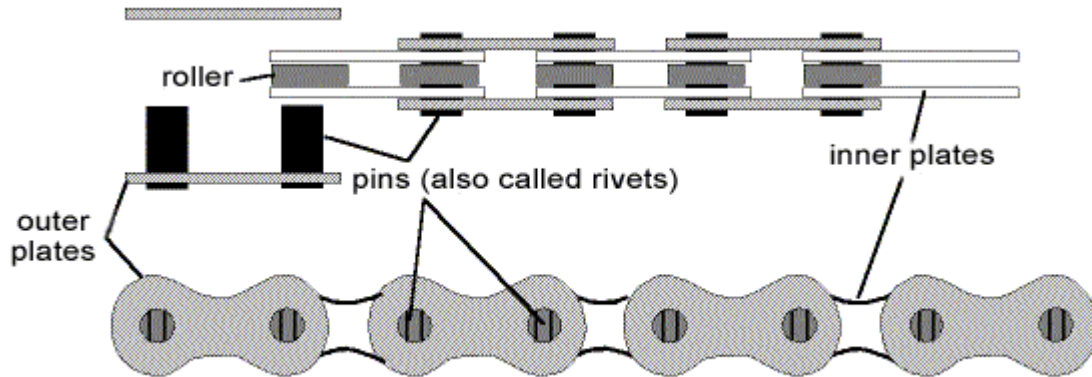


Figure 1.6: Schematic of a chain link assembly. Four major parts are shown: the outer plates, pins, inner plates, and rollers.

This means each chain segment, or link, consists of eight separate components and six moving contact points. Apply this to an average chain length of 57 links for a mountain bike and it sums to 456 separate components and 342 moving parts, more than the rest of the bike combined.³ To add another layer of complexity, all of these moving parts are directly exposed to the elements such as water, dirt, and small rocks.

Various chain designs exist to both add protection and reduce friction, but none eliminate the importance of lubrication.

Similar chains are widely used in industrial applications, leading to a substantial amount of literature on the subject. However, industrial chains tend to operate under more favorable conditions than their bicycle counterparts (e.g. coplanar sprockets, enclosed lubrication, and steady state operation), resulting in higher transmission efficiencies.¹² To give some insight into the forces involved in an actual bicycle chain, M. D. Kidd and colleagues at Heriot-Watt University in Edinburgh performed loading experiments and published their findings in their 1999 article “Experimental Examination of Bicycle Chain Forces.” Another group lead by James B. Spicer at Johns Hopkins University extended these results to include efficiency data in their 2001 article “Effects of Frictional Loss on Bicycle Chain Drive Efficiency.” The results presented in these publications were used to derive an equation for the power loss due to friction in a bicycle chain.

Friction occurs primarily at the points of contact between the roller and two inner plates with the connector pin of the chain link. In basic mechanics, it is stated that the energy loss due to friction is simply the friction force multiplied by the distance traveled ($F_F \cdot d$). From equation 1.1, we know the force due to friction is equal to the COF multiplied by the normal load, making the energy loss as follows:

$$E = \mu F_N \cdot d \quad (1.6)$$

Equation 1.6 can be extended to power loss by substituting a velocity in for the distance. For a bicycle chain, this would be the velocity of the rollers as they travel around the sprocket. The chain links experience varying normal loads as they travel around the sprocket, which also must be taken into account for this calculation. For

simplification, we will consider the total normal load equal to the sum of the maximum and minimum normal load imposed on the chain links, which occurs as a link enters the sprocket and when it is positioned at the apex of the sprocket, respectively. See Figure 1.7 for an illustration of this process. Using this information, we can now apply Equation 1.6 to the power loss due to friction in a bicycle chain:

$$P = \mu(F_{N,max} + F_{N,min}) \cdot V_R \quad (1.7)$$

The COF is specific to the lubricant used, and was measured experimentally for this study. The following section includes derivations for calculating the roller speed (V_R), as well as the maximum and minimum normal loads. Credit for the derivation of roller speed goes to Bill McKechnie from the University of Delaware.

While in operation, the rollers only move in the time it takes to enter and leave the chainring or sprocket. In this time the chain bends to conform to the geometry of the sprocket. While the roller is in any other position along the chain, the velocity is assumed to be zero. The first step is to calculate the speed of a given point on the chain, given by the following:

$$distance/min = \pi\omega D_f \quad (1.8)$$

Here the distance the chain moves per minute is calculated by multiplying the circumference of the front sprocket (πD_f) and the crank speed in revolutions per minute (ω). The next step is to calculate the length of a single chain link. This can be done by dividing the length of chain attached to the sprocket by the number of occupied teeth on the sprocket. Since about one half of a given sprocket is occupied by the chain at any given time, the length of a single chain link L_c is given by:

$$L_c = \frac{\frac{1}{2}\pi D_r}{\frac{1}{2}R_T} \quad (1.9)$$

Where D_r is the rear sprocket diameter and R_T is the number of rear teeth. With the information provided by Equations 1.8 and 1.9, a proportion can be written relating the total distance traveled by the chain to the amount of time it takes a point to travel the length of one chain link. Recall that the roller only exhibits movement when it first enters or leaves the sprocket, and the length of one chain link is the distance the chain travels while the roller is experiencing movement.

$$\frac{\pi\omega D_f}{1 \text{ min}} = \frac{L_c}{t [\text{min}]}$$

$$t = \frac{L_c}{\pi\omega D_f} \quad (1.10)$$

Solving this proportion for the unknown time t it takes for a point to travel the length of single chain link gives Equation 1.10. Now the speed of the roller can be calculated by the following:

$$V_R = \frac{X_t}{t} = \frac{X_t\omega D_f R_T}{D_r} \quad (1.11)$$

The roller speed V_R is taken to be the roller distance traveled per tooth X_t divided by the time it takes to travel one chain link length t , found earlier. The parameter X_t was defined as half the length of the gap between successive teeth, estimated to be constant and equal to 0.632 cm. Substituting in Equations 1.9 and 1.10 results in Equation 1.11 after simplification. Here we see that the roller speed is dependent on the crank rpm, front and rear chain diameters, and number of rear teeth.

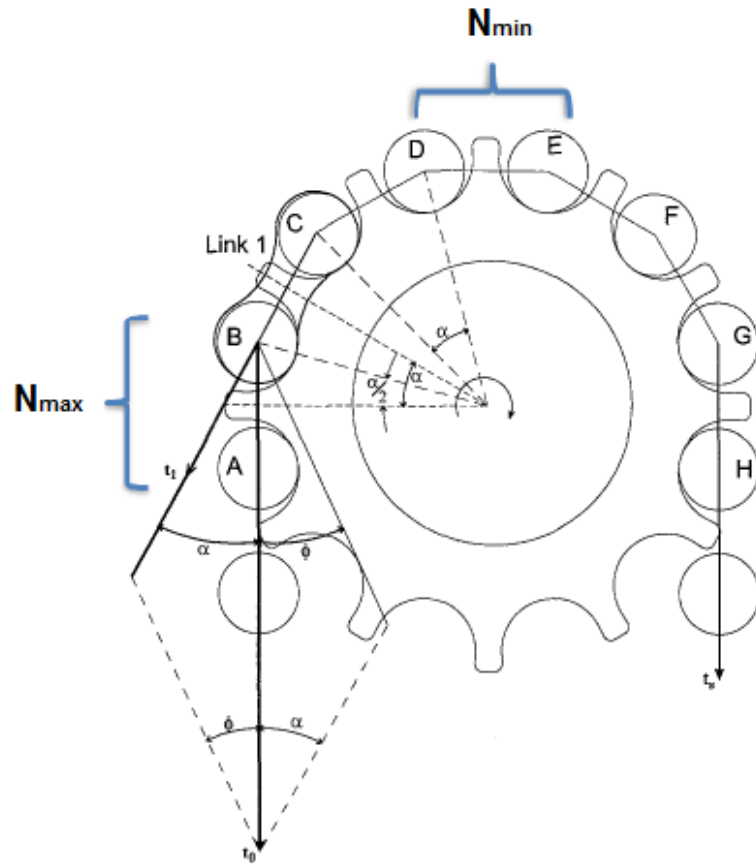


Figure 1.7: Example chain and sprocket system. Relevant angles are labeled along with the links subject to the maximum and minimum normal loads.

The maximum and minimum normal loads can be calculated using the following equations presented by Kidd, et al. which were derived based on the angle of rotation and tension in each link segment as the chain moves around the sprocket. (See Figure 1.7 for details.) First the average tooth pressure angle ϕ and articulation angle α must be calculated using Equations 1.12 and 1.13, respectively. Values are given in degrees and N_T is equal to the total number of teeth on the sprocket.

$$\phi = 35 - \frac{120}{N_T} \quad (1.12)$$

$$\alpha = \frac{360}{N_T} \quad (1.13)$$

The tension in each segment can then be calculated using Equation 1.14. This value is taken as the normal load imposed on the system.

$$T_n = T_0 \left\{ \frac{\sin \phi}{\sin(\alpha + \phi)} \right\}^n \quad (1.14)$$

The small n in this equation refers to the sprocket or tooth number, starting at zero for the first occupied link in the sprocket (link AB pictured in Figure 1.7). The constant T_0 refers to the overall tension in the chain, which was taken to be a typical value (500 N) for bicycle chains. With this numbering system, the maximum normal load occurs at link one and the minimum load occurs at the number of occupied links divided by two. Now we can use the above equations to write explicit equations for the maximum and minimum normal loads. Converting to radians for convenience, the forces experienced in the rear sprocket can be written as follows:

$$N_{max} = T_0 \left\{ \frac{\sin\left(\frac{35\pi}{180} - \frac{2\pi}{3R_T}\right)}{\sin\left(\frac{2\pi}{R_T} + \frac{35\pi}{180} - \frac{2\pi}{3R_T}\right)} \right\} \quad (1.15)$$

$$N_{min} = T_0 \left\{ \frac{\sin\left(\frac{35\pi}{180} - \frac{2\pi}{3R_T}\right)}{\sin\left(\frac{2\pi}{R_T} + \frac{35\pi}{180} - \frac{2\pi}{3R_T}\right)} \right\}^{\frac{R_T}{2}} \quad (1.16)$$

Now all the required equations for calculating the power loss due to friction in a bicycle chain have been detailed. This will be important for distinguishing the tested lubricants not only by their COF and rate of wear, but by their actual performance in a bicycle drivetrain as well.

Chapter 2

EXPERIMENTAL METHODOLOGY AND CONSTRUCTION OF THE TRIBOMETER APPARATUS

2.1 Experimental Details

The primary device used to measure friction and wear is a tribometer, which consists of two surfaces that are placed in contact and allowed to move or slide past each other. Tribometers are often referred to by the specific contact arrangement they simulate. For this study, a pin-on-disc tribometer was used to best simulate the conditions and motion associated with a bicycle chain. This particular device consists of an exposed ball bearing (in this case the “pin”) that is placed in contact with a flat surface protected by a layer of the lubricant being tested. A motor spins the disc, producing a friction force that pushes the bearing in the direction of motion. Figure 2.1 shows a schematic of this process. By recording the applied normal force and force due to friction, the coefficient of friction can be measured. The COF is a measure of the relative performance of the lubricant; a lower COF is desired as it means the lubricant effectively reduces the friction force when the surfaces are in motion. The experiments in this study were set up to run at forces and speeds that are comparable to those seen in a bicycle chain under operation. Multiple data points for the COF with each lubricant were recorded at speeds at regular intervals ranging from 20 mm/s to 220 mm/s. The normal load was maintained relatively constant at values ranging from 180 - 220 millinewtons (mN).

The test can also be run for an extended period of time, after which the amount of material displaced from the plate, called a wear track, can be measured. Decreased wear and better lubricant performance correspond to a smaller wear track after a set time period. Wear measurements have the tendency to be sensitive to a number of

factors, which must be kept consistent throughout all experiments to obtain meaningful data. Variables that can affect the rate of wear include the normal load, speed, length of time, roughness of the two contacting surfaces, amount of lubricant, temperature, pressure, and humidity. Convenient control values were chosen for these experiments based on some preliminary results. Tests were run for one hour each, under a constant normal load of 1500 mN at ambient temperature and pressure. All experiments were done using $\frac{1}{4}$ " diameter stainless steel ball bearings in contact with a stainless steel plate polished to a uniform roughness. The resulting wear track was then measured at different points along the circular track using an interferometer.

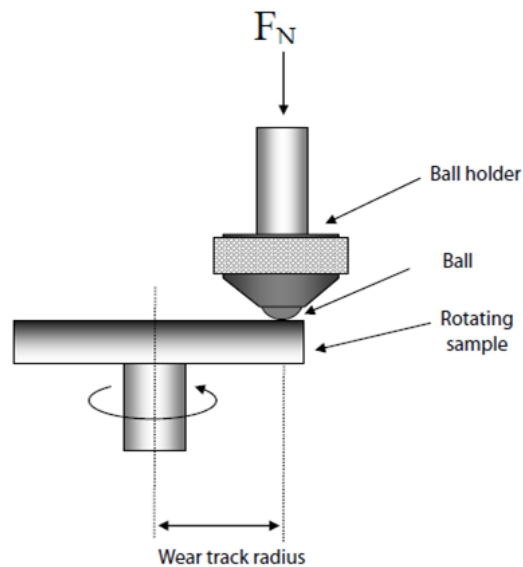


Figure 2.1: Schematic of a pin-on-disc tribometer. A normal load is applied to a holder containing a ball bearing that is placed in contact with a rotating sample.

An interferometer measures the power and spatial distribution of the interference pattern produced by a beam of light that is reflected and recombined to accurately and precisely measure very small distances. The overall shape, width, and depth of the wear tracks produced in these experiments were measured using this technique to an accuracy of a fraction of a nanometer. Wear data was collected using the assumption that the wear track was in the shape of a perfect triangle dug out from the surface. The wear was calculated as the area of the triangle and was reported as the average area of material lost around the track in square microns. Figure 2.2 provides a sample wear track as seen when placed under the interferometer.

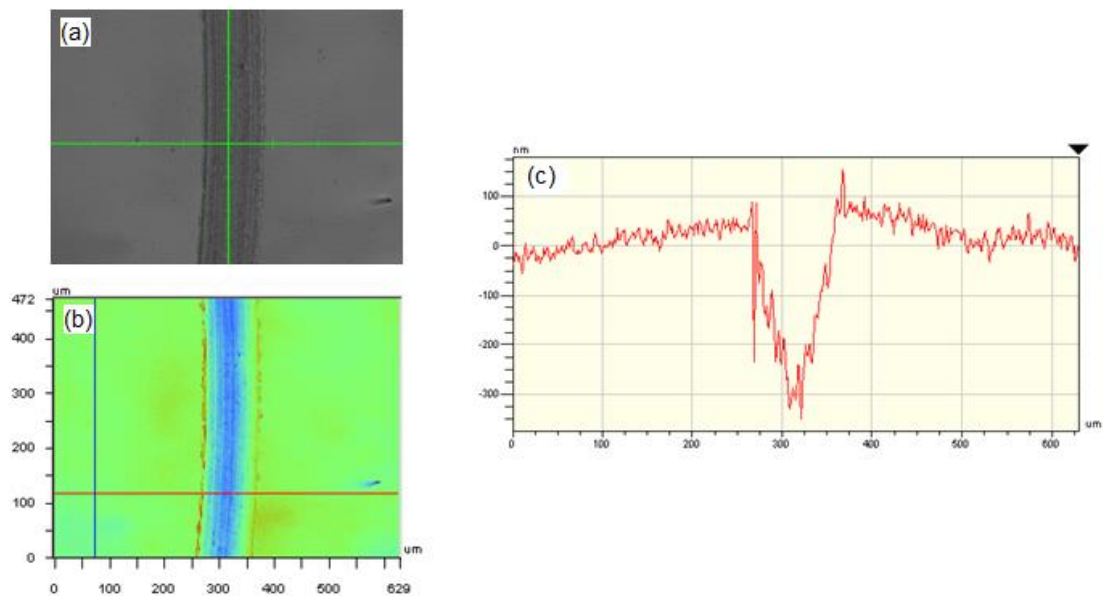


Figure 2.2: A sample wear track is shown. The track under the interferometer before scanning (a). The color coded track after scan. Blue represents valleys and peaks are shown in red (b). Track profile showing a clear width and depth. Area was calculated using these images (c).

2.2 Tribometer Design

Initially, the measurements presented in this paper were taken with a borrowed pin-on-disc tribometer set up in the tribology lab. However, this equipment was needed for another project, so we took on the challenge of constructing a new tribometer specific to our research project. Designing a new piece of equipment always poses a number of challenges and specifications that need to be met. For our purposes, the tribometer had to spin a sample disc, raise and lower a ball bearing, and be able to accurately apply and measure both the normal force and friction force. Precision and reproducibility are of utmost importance when making friction and wear measurements. Therefore, the final product had to be simple to use and easily maintained, calibrated, and adjusted. The goal was to produce a self-contained, user-friendly prototype capable of making the necessary friction and wear measurements. This section details the design process of each component of the tribometer along with models and pictures of the different components. Detailed SolidWorks drawings of the individual parts are included Appendix B.

The first feature that was designed was the mounting stage for the motor and spindle system that drives the disc. The stage was cut from solid aluminum and measures 6" x 12" x 0.5". Four aluminum legs attach via bolts onto the sides of the stage and lift the platform about 6" off the ground. The legs were also drilled and tapped at the bottom to fit adjustable rubber grips that aid in leveling the stage and reducing the effect of vibrations in the workbench. The motor that was chosen for this application is the MDrive 34 Plus Speed Control electric motor from Schneider Electric. A smaller model could be used; however we wanted to ensure the motor produced sufficient torque and had a high range of speed. The motor is mounted

spindle side down in an aluminum casing beneath the stage and is powered by an enclosed 48V direct current power supply mounted on the side of the stage.

The front end of the stage was cut to produce a 2" diameter hole to accommodate the spindle housing and sample disc. The spindle housing is made of aluminum and bolts to the top of the stage via a flange connection. This housing contains two angular contact bearings positioned about 2" apart from each other at the top and bottom of the cylinder. The spindle itself is a stainless steel rod 5" long and 0.5" in diameter that is press fit through the bearings. Angular contact bearings perform best when under both axial and radial load. To achieve this, an axial load was manually applied by squeezing the assembly along the axis of the spindle shaft with a sliding ring pressed against a wave spring in contact with the bottom bearing. The ring was then secured in position with a set screw to maintain the axial load on the bearings. Radial load on the bearings results from tension in the timing belt attached to the motor. The end of the spindle extends approximately 4" below the stage with a timing pulley mounted at the bottom. This is connected to a larger pulley on the motor by a rubber timing belt. Tension is applied to the belt by manually sliding the bottom platform of the motor casing away from the spindle and tightening it in place. The motor input voltage to disc rpm conversion was calibrated using a tachometer and programmed into LabVIEW for easy control over the speed and direction of rotation.

The sample disc measures 4" in diameter and is fitted on the end of the spindle above the stage with a set screw. This serves as the platform for holding the steel plate and lubricant sample, which is secured with an aluminum housing cover attached to the disc with removable socket cap screws for easy cleaning and sample changing. The polished steel sample plates are squares measuring 1.5" by 1.5" and are 0.125"

thick. These are placed in the housing with a wave spring or rubber O-ring underneath to press the top of the plate flush against the housing, preventing any lubricant run out and helping to dampen any inertial forces in the ball. The spindle and disc are both machined out of 304 stainless steel to better resist deformation due to loading and temperature changes. A 3D rendering of these components as well as a photo of the completed drivetrain system are given in Figure 2.3 below.

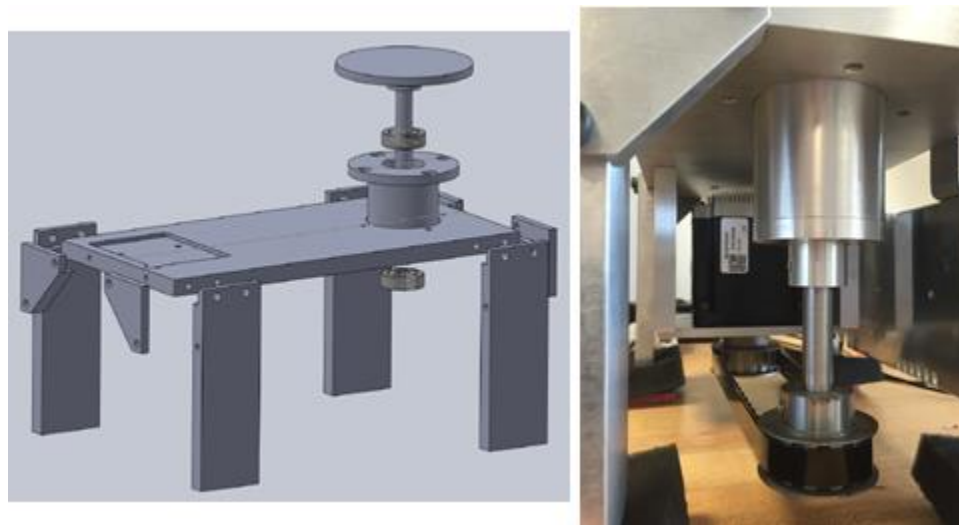


Figure 2.3: Three dimensional CAD model of the stage and spindle system (a). Photo of the completed drivetrain system, including the motor, pulleys, and timing belt (b).

The stage, sample housing, and drivetrain system is now complete, allowing for the arm and ball holder components of the tribometer to be designed. These components must be able to be adjusted precisely in at least two directions: up-down (z) and forward-reverse (x). Left-right adjustment is possible but unnecessary, as these components are designed to be locked into place at the center of the stage. To achieve

these movements, three different manual positioner micrometer stages were purchased. The x-axis stage allows for adjustment of the ball forward and back, to specify the desired wear track radius. The z-axis stage is capable of raising and lowering the assembly for the loading and unloading of the ball and sample plate. Lastly, a tilt stage was fitted between the x and z-axis stages for leveling the assembly and ensuring proper loading. These three stages, pictured in Figure 2.4, form the backbone of the assembly, attaching the arm and ball holder components to the top of the stage.

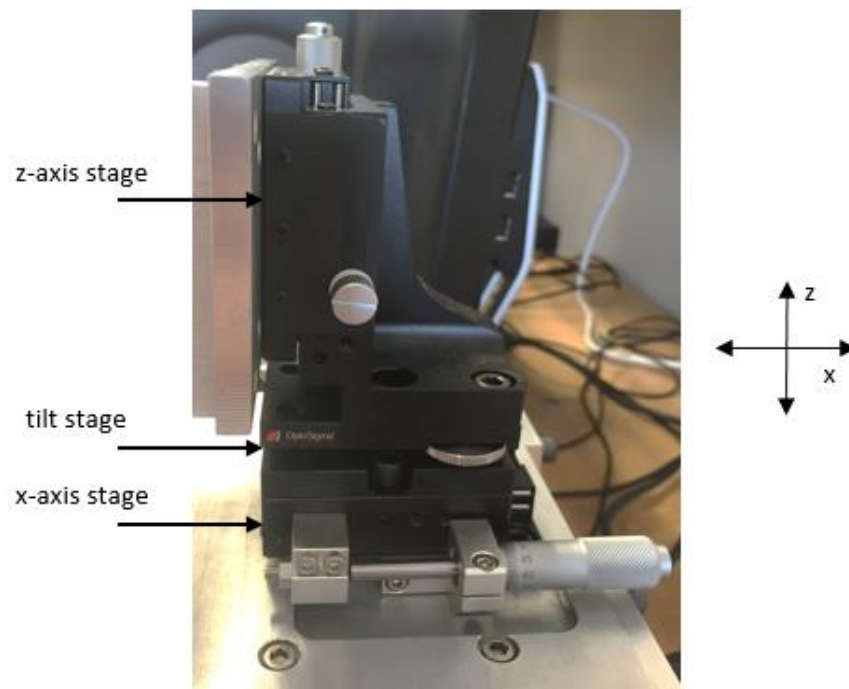


Figure 2.4: Adjustable roller stage assembly. From bottom to top: x-axis stage, tilt stage, z-axis stage.

The arm itself was perhaps the most difficult component of the entire apparatus to design. It took several stages of development and many trial-and-error tests to reach the current design. The difficulty lies in the fact that the arm and sensor combination must be capable of measuring the normal force and friction force simultaneously, while maintaining a minimal level of vibration and noise to achieve the necessary level of precision needed to make an accurate measurement.

With the goal of simplicity in mind, it was decided that only one sensor was required. This would measure the friction force, while the normal force would be controlled by a dead-weight loading system. A mass can simply be placed onto the arm, and its corresponding weight will be equal to the normal load on the ball. Measuring the friction force, however, turns out to be slightly more complicated. One method is to measure the deflection of the arm when the disc is in motion with a displacement sensor, and generate a calibration curve to calculate the corresponding friction force. A larger friction force will result in greater deflection of the arm and a greater signal coming from the sensor. The COF can then easily be calculated by dividing this value by the known constant normal load.

Going forward with this method, before a sensor is even chosen, the arm must be able to perform two major functions: deflect enough to produce a measurable and distinguishable signal between different lubricants, and be designed such that a mass can be easily placed on the top for loading in the normal direction. To meet these criteria, a solid block of aluminum in the shape of a capital “T” was cut to form the arm. The total length of the block measures 5.75” with a width of 1.0” and a uniform height of 0.75”. The arms of the “T” extend out 0.5” on either side of the base. The

length of the block was designed such that the longer end reaches over the center of the sample disc when mounted to the adjustable stage backbone.

To achieve the necessary deflection a spring system was implemented at the ends of the extensions located at the back of the block using cuts of a sheet of steel shim stock. One end of each sheet cutout is secured to each side of the arm extensions, while the other sides are secured to two smaller L-shaped arms mounted of either side of the main arm. The steel shim stock comes in a wide variety of thicknesses, which correspond to the magnitude of the spring constant in this case. Sheets with thicknesses ranging from 0.005" to 0.032" were purchased and cut to produce many rectangular springs measuring 0.5" by 3". The springs are secured to each arm with small rectangular aluminum covers, cut 0.125" thick with socket cap screw holes on the four corners for tightening over the steel sheets. Depending on where the springs are secured the length free for movement can also be adjusted, further increasing the level of control over the spring constant. The L-shaped flexure arms were designed to be 2.75" long, providing significant room for this adjustment. The goal is to find the optimal spring stiffness for the chosen displacement sensor, such that a wide range of signals can be recorded without maxing out the sensor. Figure 2.5 provides a three dimensional model and labeled diagram outlining the different components as initially designed.

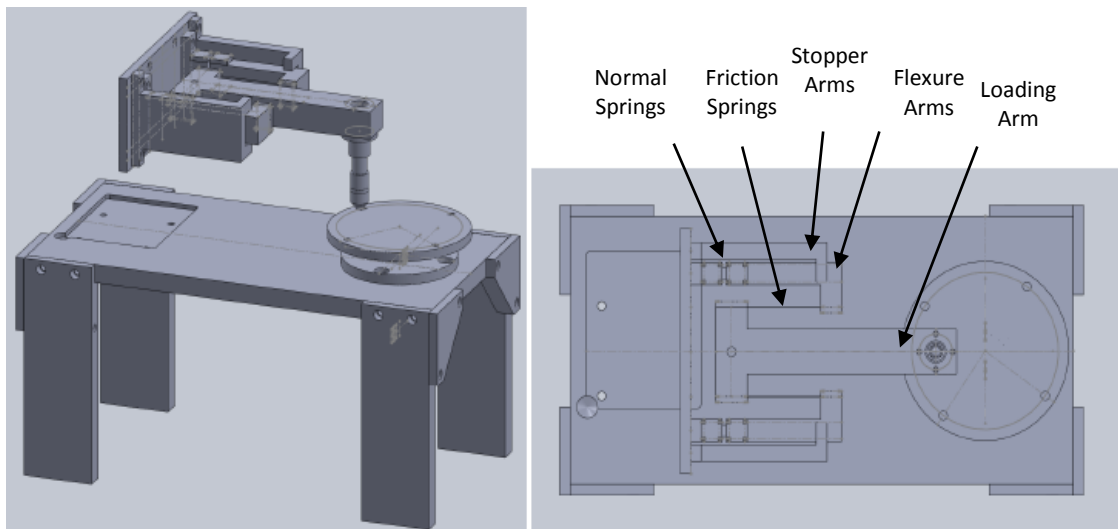


Figure 2.5: Side and top views of the load arm and spring system. Major components and flexures are labeled accordingly

Similar springs were also used to allow for deflection in the z-direction, to allow for leveling and proper loading in the normal direction. These were cut from the same sheets of shim stock, however they measure only 0.25” by 1.0” and had to be thicker to support the full weight of the arms. These were secured to the tops of the two flexure arms and anchored to extensions on the back mounting plate via the cover plates detailed earlier. The back mounting plate attaches directly to the z-axis stage, allowing the entire assembly to be raised or lowered together. Counter weight is added onto a threaded rod that connects to a hole in the back end of the loading arm and extends up and out over the adjustable stage backbone. This is to help balance the weight of the arms themselves, leveling out the assembly and reducing the stress on the normal axis springs. To prevent these springs from over extending during loading

and unloading, two stoppers were machined to wrap around the flexure arms with a clearance of a few millimeters above and below the arms. Figure 2.6 shows a photo of the completed system.

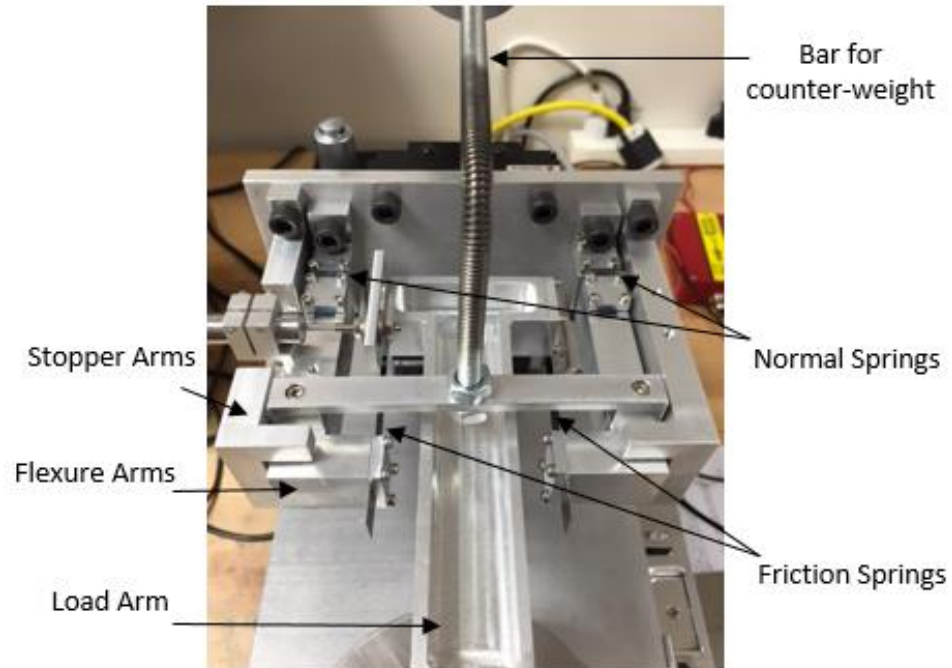


Figure 2.6: Close up photo of the finalized arm and spring system.

As can be seen in Figure 2.5, a small hole was cut through this end of the arm to accommodate the ball bearing holder. The holder originally consisted of a 1.5" long stainless steel chute that attached to the end of the arm and extended down above the sample plate. After implementation, however, it was found that this design was too heavy and was contributing to oscillations in the flexure springs, resulting in increased

signal noise. To correct this issue a new part was made that operates on the same principal as the flexure springs, pictured in Figure 2.7.

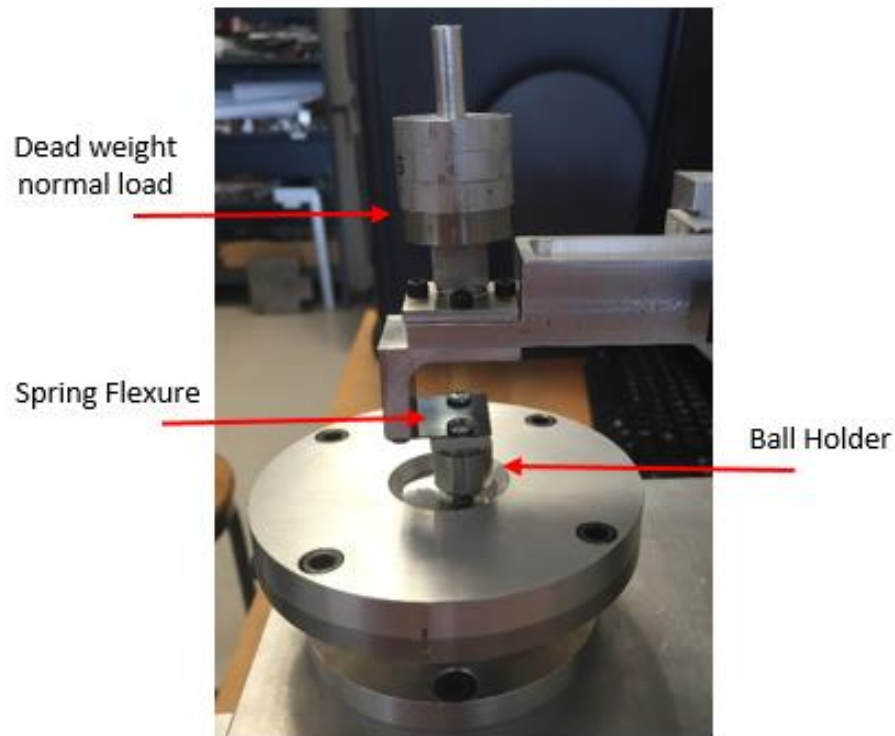


Figure 2.7: Final ball bearing holder design. Masses for applying normal load are placed around the rod at the end of the load arm.

An aluminum bracket was machined to attach to the bottom of the load arm was fitted with a piece of the same spring steel material used for the flexures. This spring extends over the sample plate and a small ball catch is attached to the bottom, holding the bearing in contact with the plate. In this design the spring can flex up and down as the ball slides over plate, helping to dampen any inertial forces in that

direction. The ball catch is threaded on the inside so that it can be removed and reattached from a screw mounted at the bottom of the steel spring, making the ball bearing easily accessible for cleaning or replacement. The top of this bracket was also machined to have a rod coming out of the opposite end for the placement of ring-shaped masses. These masses were machined to precise dimensions out of aluminum and stainless steel to apply the desired normal load for each experiment.

Many different types of sensors are currently available for measuring displacement, but it must be considered that the size, shape, and material of the arm, spring stiffness, and the placement of the sensor will affect the sensitivity of the measurements. This poses a crucial design question: what type of sensor should be used, and how should it be implemented?

The initial decision was to use a capacitance sensor to measure displacement, since there were some in the lab that were currently not in use. Capacitance sensors work on the principal that the capacitance between the sensor and target is a function of the distance between the two surfaces in a homogenous electric field. These devices are extremely precise and can readily detect distances in the sub-micron range.⁶ However, the models available in the lab had a measurement range of $\pm 50 \mu\text{m}$, which is extremely small and required a very high spring stiffness to prevent the sensor from maxing out during experimentation. The other major problem with this sensor was the alignment. For an accurate and reliable measurement, the capacitance probe had to be perfectly aligned with its target at just the right distance. Since the gap is only 50 microns, this proved to be very difficult to do with the current setup, as the gap is not easily visible with the naked eye. This means there is no guarantee the sensor was

properly aligned and could easily become misaligned again due to contact with the target during the course of a calibration or experiment.

The second option considered was a linear variable differential transformer (LVDT). These sensors consist of a stationary shell and magnetic iron core that can slide back and forth through the shell. The shell contains three solenoidal coils: one primary center coil and two outer coils. Current is driven through the center coil, causing an induction current to be generated at the other two coils. A displacement of the core in one direction in turn causes the voltage in one secondary coil to increase while the other simultaneously decreases.²⁰ The LVDT outputs this difference in voltage between the two outer coils, which is then calibrated to a distance, or in our case, the friction force.

A new unguided LVDT and amplifier combination was purchased with a range of ± 0.65 mm (± 650 μ m) and a linearity error of $\pm 0.5\%$. This tolerance is 13 times greater than that of the capacitance sensor, which allowed for much easier alignment and calibration. The shell component was mounted on one of the flexure arms and the core was attached to a target positioned above the loading arm, as shown in Figure 2.8.

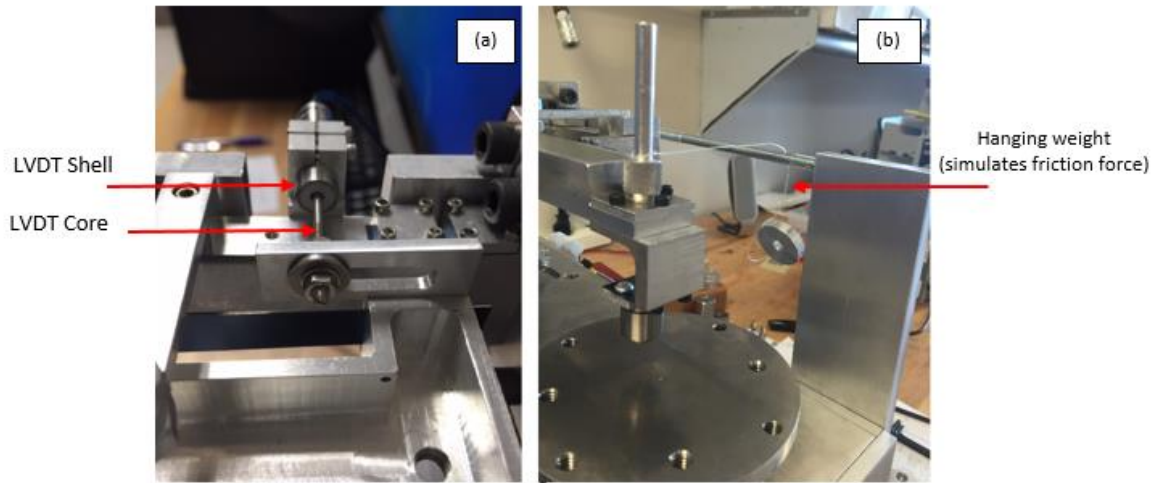


Figure 2.8: LVDT alignment and calibration method. The shell mounts to the side flexure arm while the core attaches to a target on the load arm via a nut and washer (a). Various masses are tied to the load arm and hung over a smooth cylinder with fishing line to exert a lateral force, allowing the output voltage to be calibrated to the friction force (b).

Since the entire apparatus moves together, the core maintains alignment at all times and will slide in and out of the tube as the springs flex and the arm is deflected in one direction or another depending on the direction of rotation of the disc. The calibration was carried out by plotting the sensor's output voltage against the friction force. The friction force was estimated by tying weights to the end of the loading arm with a monofilament cable (fishing line) and hanging them over a smooth cylinder suspended to the side of the arm. Assuming no friction on the cable, the weight suspended over the cylinder deflects the springs the same amount as a true friction force of the same magnitude, meaning the calibration can be done from voltage straight to friction force. The resulting calibration curves for two different spring thicknesses are given in Figure 2.9.

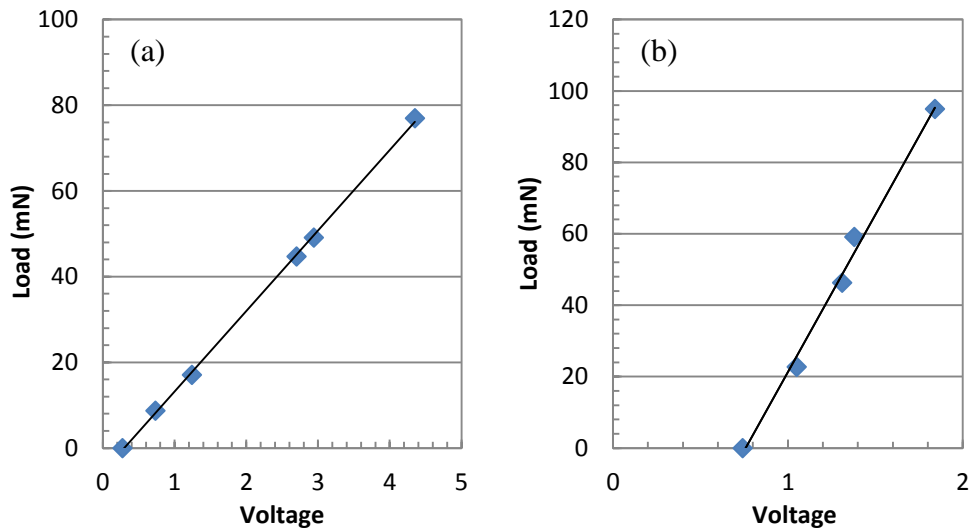


Figure 2.9: Calibration curves to convert LVDT output voltage to the friction force for spring thicknesses of 0.006" (a) and 0.010" (b). Calibration constants are taken as the best fit slopes of 18.78 mN/V and 88.05 mN/V, respectively.

During the course of testing and troubleshooting the new tribometer, some improvements were made to improve its practicality and performance. First, the solid aluminum loading arm was unnecessarily heavy and cumbersome, preventing significant deflection in the springs due to friction. Consequently, the arm was hollowed out leaving only 0.125" thick walls around the edges to aid in lightening the assembly. Another problem was that the two auxiliary flexure arms were not moving in unison, causing lopsided motion and buckling when in use. This was corrected by adding a simple connector bar between the two arms, locking them into uniform motion and distributing the load evenly. To further reduce the self-weight of the loading arm, the counter-weight bar was moved to this connector, transferring the weight from the loading arm to the flexure arms. The stopper arm on the side on which the sensor was mounted was also altered to include a cutout allowing the sensor to

stick out from its position on the flexure arm. With these improvements and further testing it was found that the optimal spring thickness and length for calibration with the LVDT were 0.010” and 1.5” respectively. The completed tribometer after improvement and optimization is pictured in Figure 2.10.

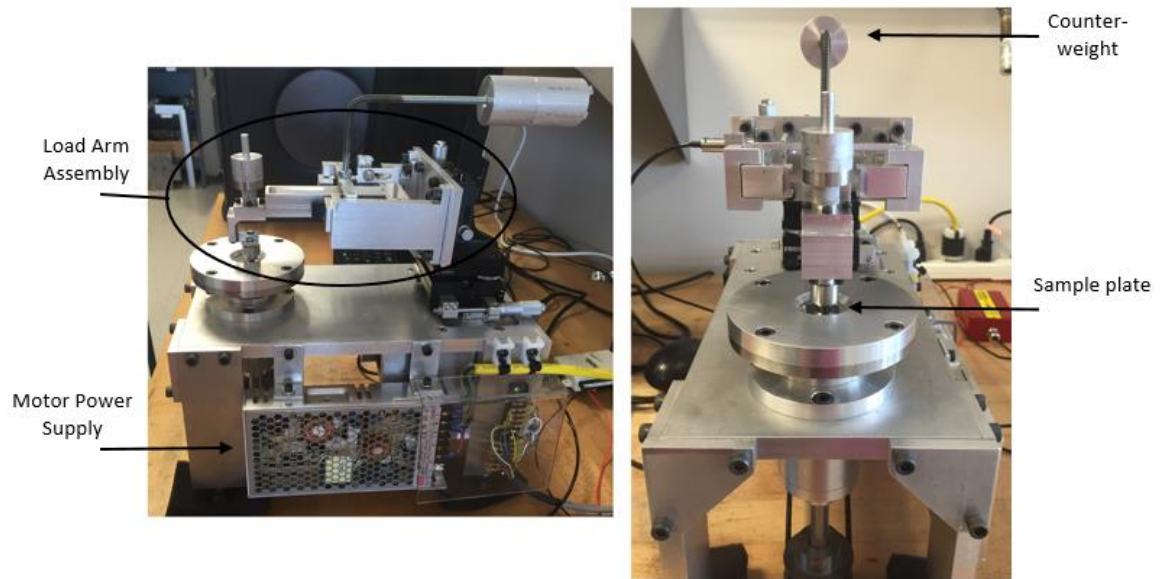


Figure 2.10: Profile and front views of the completed tribometer after troubleshooting and optimization.

Chapter 3

FRICITION AND POWER LOSS RESULTS

The coefficient of friction was measured for a number of lubricants from speeds ranging from about 20-125 mm/s to see if there was any relationship between the COF and the sliding speed. Figure 3.1 shows the COF values for a selection of these lubricants. Table A.1 in Appendix A contains all of the lubricants tested with their respective sample abbreviations.

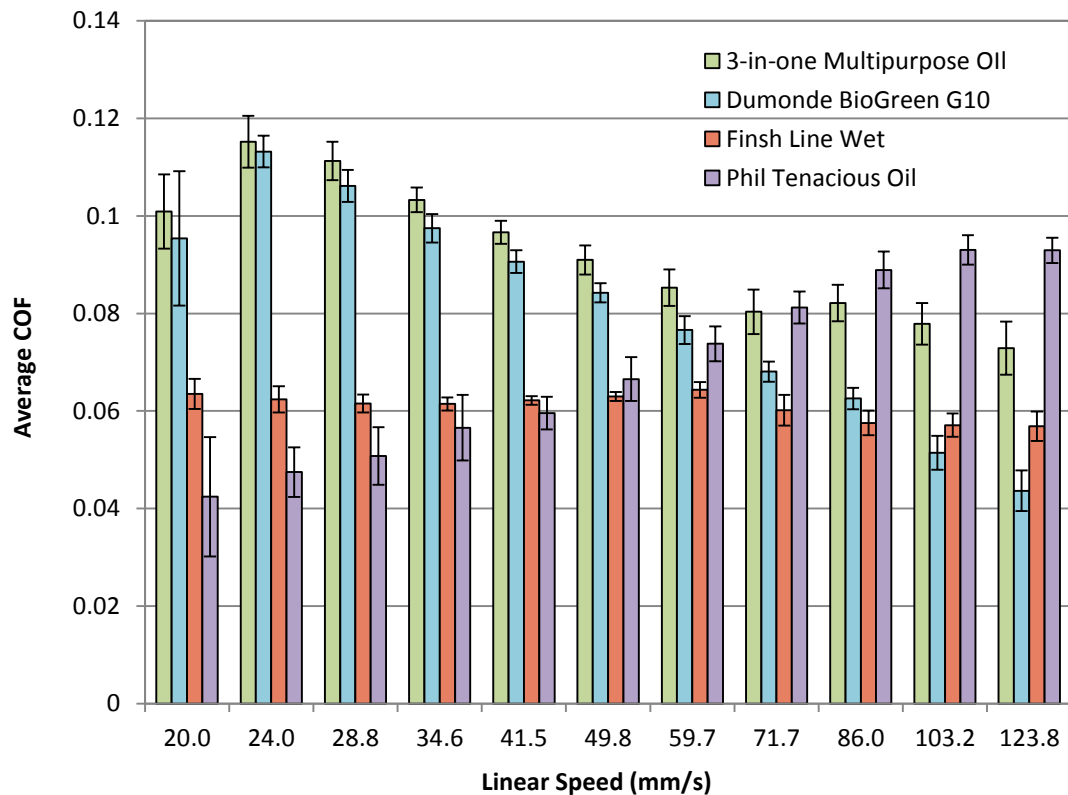


Figure 3.1: Selected lubricant COF values over a range of linear speeds. Error bars equal to the standard deviation for each lubricant are shown.

The lubricants shown in Figure 3.1 were chosen because they are a good representation of the overall results for COF vs. speed. The relationship can vary greatly based on the lubricant. For some samples, the COF had a clear decreasing trend with increased speed. Conversely, the COF increased with speed for some lubricants, and for others the COF remained relatively constant across all speeds. These different effects can be explained by the various lubrication regimes described in Chapter 1.

The most common trend was for the COF to remain relatively constant at lower speeds before beginning to decrease at higher speeds, which is consistent with a Stribeck Curve similar to the one pictured in Figure 1.4. At low speeds, boundary lubrication is maintained resulting in a constant COF. As speed is gradually increased, the lubrication enters the mixed regime, which is characterized by a sharp drop in friction. If we continued to increase speed during our experiments, it would be expected that the COF would reach a minimum value before beginning to increase, as hydrodynamic lubrication starts to occur. This is likely the scenario for the lubricants which saw a consistent increase in friction. High viscosity lubricants can reach the hydrodynamic regime at lower speeds, allowing viscous forces to cause increased drag on the ball bearing as speed increases. This was confirmed with an experiment using glycerol as a lubricant. Glycerol has a very high viscosity (1200 cP, more than 1000 times greater than water) and showed a clear increase in friction at higher speeds. The lubricants for which the COF remained relatively constant over the range of speeds likely stayed in boundary lubrication for the duration of the test.

In addition to testing common synthetic and natural oils, the coefficient of friction was measured for a selection of commercial bicycle chain lubricants currently

available on the market. This was done to compare different products as well as to determine a performance standard for future experimental samples. The reported values for the COF are taken from the 123.8 mm/s linear speed tests, as this was the closest value to the value estimated for a typical roller sliding speed on a bicycle chain. To analyze the relative performances between different lubricants, values were chosen for the front and rear sprocket diameters, as well as the rider cadence (crank rpm). The front sprocket diameter was set as 18.6 cm (52 teeth) and the rear diameter was set as 6.9 cm (21 teeth). A rider cadence of 90 rpm was assumed. These results are included in Figure 3.1, which shows the power loss plotted along the left axis and COF along the right axis.

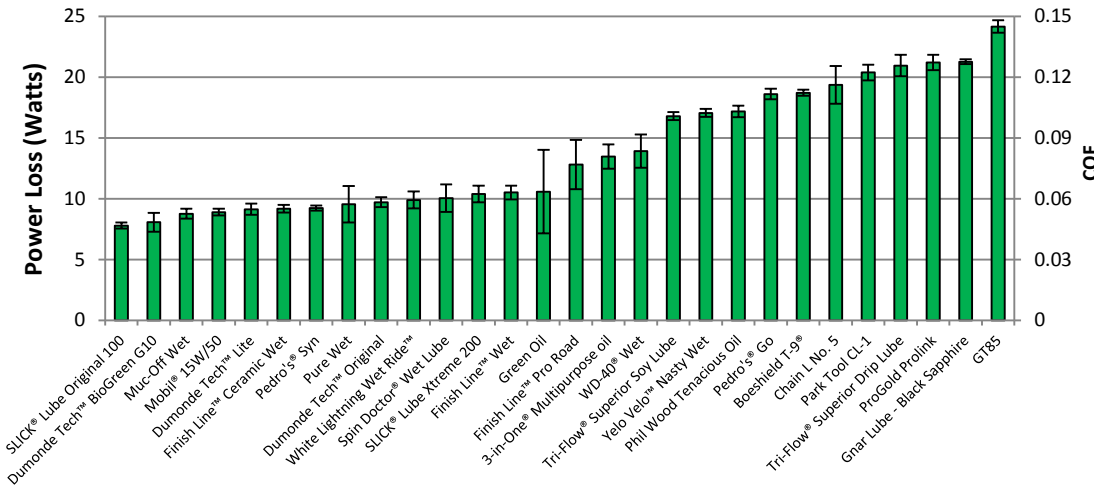


Figure 3.2: Coefficient of friction results and corresponding power loss values for common bicycle chain lubricants.

As can be seen from Figure 3.2, there is a broad range of performances between the different lubricants. The best performing lubricants scored below 10 watts lost, or a COF of about 0.06, while the worst performers had greater than 20 watts lost, or a COF of about 0.12. Using this information some calculations can be done to relate these results to the performance of an actual cyclist. It was found that every watt of power lost to friction in the drivetrain corresponds to a decrease in speed of about 0.05 km/h, assuming a 70 kg rider with average cycling ability and a constant power output. Since the difference in power loss between the best and worst lubricants is about 10 watts, this results in a 0.5 km/h difference in speed just by choosing a different lubricant. In a 40 km time trial, this would translate to a 45 second difference in finishing times, which is highly significant, especially for competitive cyclists.

Another set of experiments included measuring the COF for various natural oils, such as canola oil, castor oil, and soybean oil. This was done to test these products for their efficacy as a lubricant to possibly use as the base component in a finished lubricant product. Figure 3.3 shows the results of these tests, again reporting the COF at 123.8 mm/s.

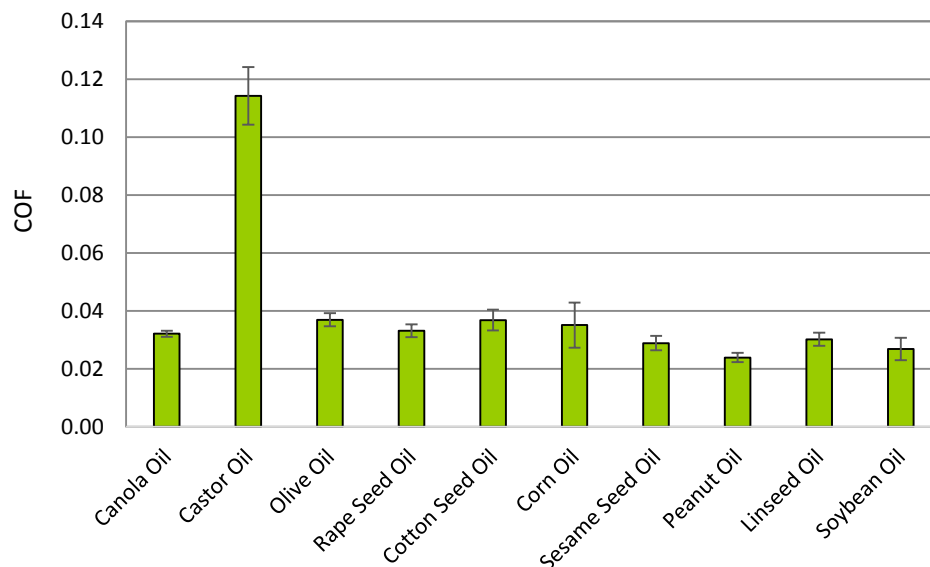


Figure 3.3: Coefficient of friction values for various natural oils.

From Figure 3.3 it can easily be seen that these oils perform very well in terms of reducing friction, as all the samples gave a COF of less than 0.04, with the exception of castor oil. This result can be expected, since castor oil has a viscosity of approximately 990 cP, more than an order of magnitude greater than any of the other oils. This is due to the unique composition of castor oil, which is comprised of mostly monounsaturated fatty acids (rather than polyunsaturated), resulting in the increased viscosity.⁸ These effects are discussed in more detail in Chapter 5. The COF of castor oil increased with speed for this reason, while the friction decreased with speed for the other oils. Based on these results most of the natural oils we tested would be feasible as a lubricant base. In fact, it may seem reasonable to simply apply some of these oils as a lubricant by itself. However, there is another important factor we must consider to make an effective lubricant: the wear.

Chapter 4

WEAR RESULTS

Wear was tested by the methods described in Chapter 2 for the same lubricant samples used in the friction experiments. Preliminary tests were done to determine convenient control values for the speed, load, and length of time at which each test should be run. A speed of 50 mm/s, load of 1500 mN, and time of one hour were chosen, as these values resulted in wear that was distinguishable between different lubricants without creating a wear track too large, which would increase the time needed between tests to re-polish the surface of the sample plates. Figure 4.1 shows a graph of the wear for the same 28 common bicycle chain lubricants used in the friction and power loss tests.

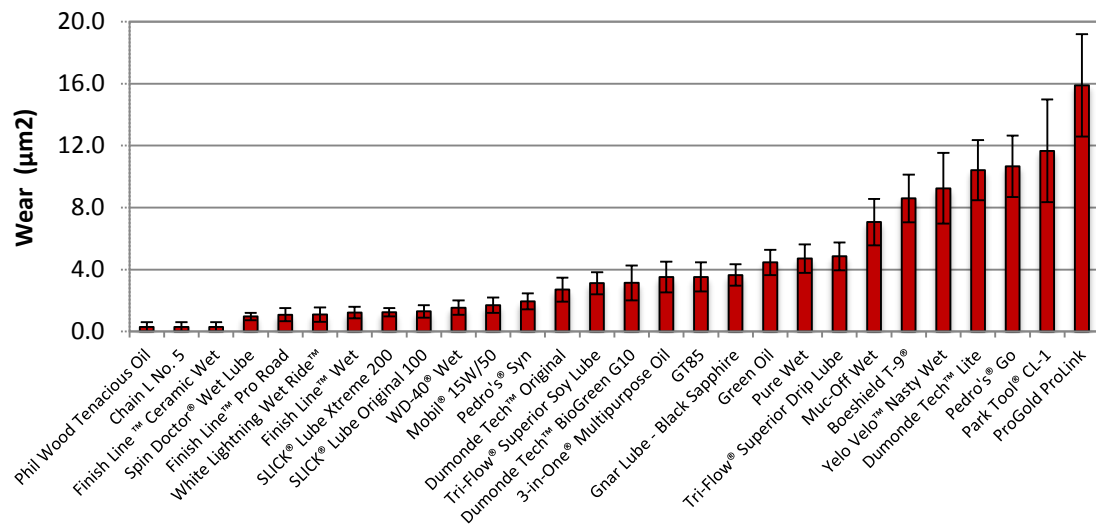


Figure 4.1: Wear results for common bicycle chain lubricants.

Here we can again see a wide range of results for the performance of these lubricants. The majority of the products maintained a relatively small amount of wear after the one hour test, resulting in a track cross section area of less than $4.0 \mu\text{m}^2$. Three lubricants including Phil Wood Tenacious Oil, Chain L No. 5, and Finish Line Ceramic Wet, gave no measureable wear after the one hour test. When the steel sample plate was placed under the interferometer following these experiments, no wear track was distinguishable from the baseline roughness of the surface. The wear increased rapidly for the poorer performers, which had more than double the wear at about $9 \mu\text{m}^2$. The worst performing lubricant, ProGold Prolink, had more than four times more wear than the better performers at $16 \mu\text{m}^2$.

Another important note about these wear results is the variability. The standard deviations were generally much larger for these experiments compared to those from the friction results. This is likely due to the wear measurements being sensitive to a large number of factors, making perfect control and reproducibility difficult.

An experiment was also done to measure the effect of an anti-wear additive on a lubricant at increasing concentrations of the additive. Pure canola oil was tested to determine a baseline wear result, then individual samples containing increasing concentrations of the anti-wear additive Lubrizol LZ4370LG were tested for the resulting wear after a one hour interval. Figure 3.2 shows the results of this experiment.

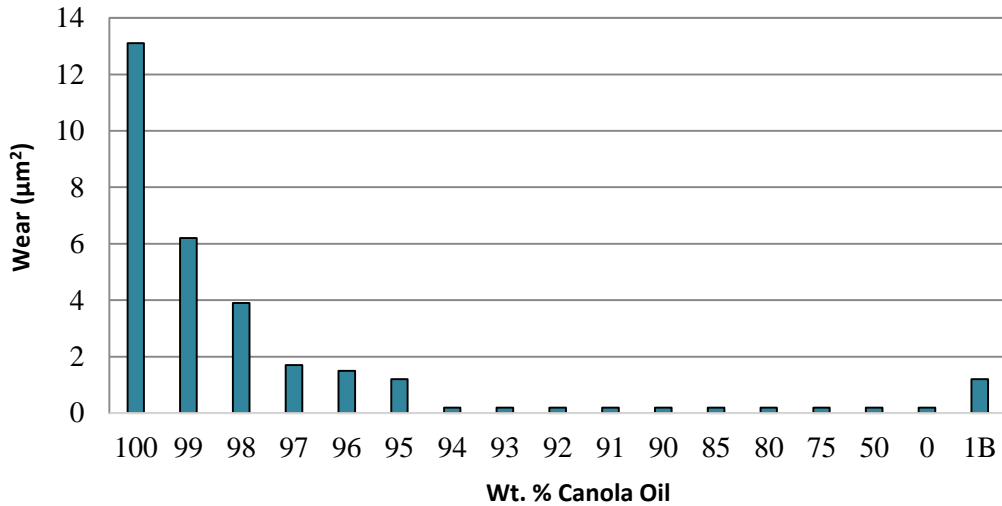


Figure 4.2: Effect of anti-wear additive (Lubrizol LZ4370LG) on canola oil base lubricant. Lubricant 1B (Slick Lube 100) is shown as a reference.

The data in Figure 4.2 show a sharp decrease in wear as the concentration of the anti-wear additive is increased. The baseline wear for canola oil was similar to the poorest performing lubricants from Figure 4.1 at about $13 \mu\text{m}^2$. By adding just 1% by weight of the additive, the measured wear decreased by a factor of more than 2. Furthermore, at 3% additive the wear drops to less than $2 \mu\text{m}^2$, and at 6% additive and greater, the wear became negligible after our one hour test. This shows that including only a small amount of additive in a lubricant can drastically effect its performance. Slick Lube 100 (sample 1-B) is formulated with 5% of this anti-wear additive, which gave a comparable result to the canola oil formulated with 5% additive.

Another interesting representation of the data is to determine if there is any relationship between the coefficient of friction and wear for the lubricants considered. Figure 4.3 shows a plot of the wear versus the coefficient of friction.

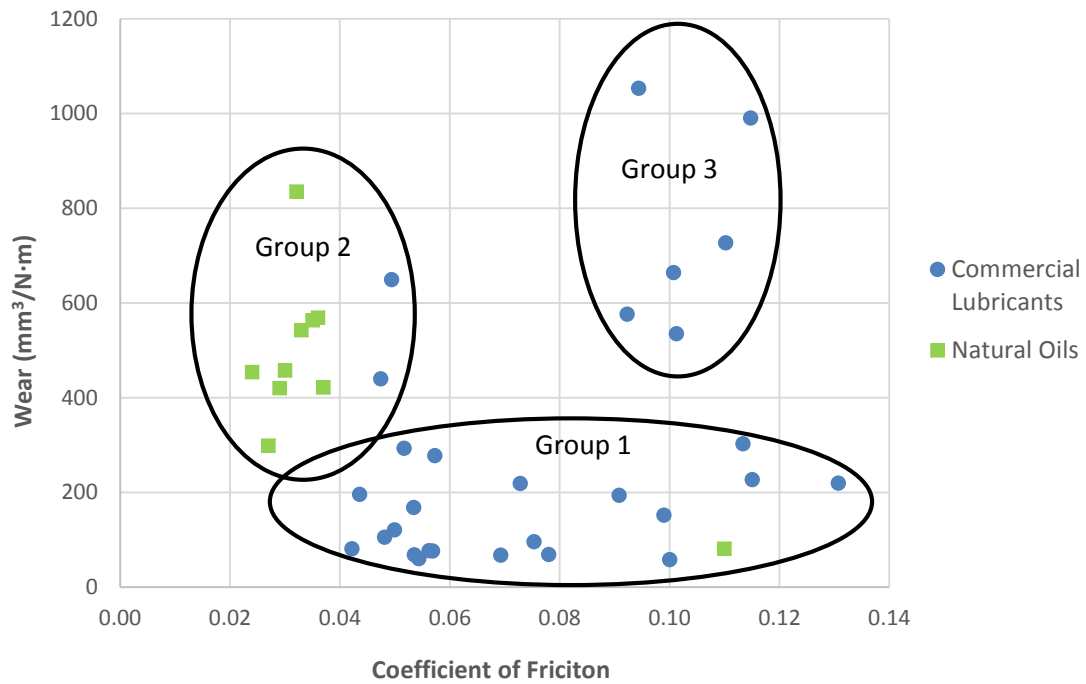


Figure 4.3: Plot of wear versus coefficient of friction for various lubricants.

Here the wear is plotted as volume lost per unit normal load per distance traveled ($\text{mm}^3/\text{N}\cdot\text{m}$) to normalize the data and fit all points on a single plot. Examining the data, there appears to be three distinct groups in lubricant performance. Group 1 includes lubricants with low wear and medium to high friction coefficients. Group 2 lubricants have low COF values but higher wear, and group 3 includes lubricants that exhibit both high friction and wear. By distinguishing between the commercial lubricants and natural oils that were tested, there is a clear difference in performance between the two categories. All of the natural oils fall under group 2, with the exception of castor oil, which falls under group 1 for the reasons discussed in Chapter 3. Although these oils perform well in terms of reducing friction, they do not produce a lasting protective barrier between the sliding surfaces, as evidenced by their

high wear values. However, this problem can be remedied by adding a small amount of anti-wear additive to the oil as can be seen in Figure 4.2. This greatly reduced the wear while leaving the friction coefficient relatively unchanged.

The commercial lubricants had a higher variability in performance, with the majority of the lubricants falling in group 1, with some samples scattered between groups 2 and 3. This is consistent with the wide range of performances in both friction and wear seen in Figures 3.2 and 4.1. Optimal performance is considered to be towards the bottom of group 2, or to the left of group 1, where both the COF and wear are at a minimum. Based on these results the top performers in both friction and wear included Slick Lube 100, Dumonde BioGreen G10, White Lightning Wet Ride, and Spin Doctor Wet Lube.

There appears to be an inverse relationship between COF and wear, excluding a few outliers. As the COF increases, the wear values tend to decrease on average. This trend can be explained by tying the results back to viscosity. As discussed earlier, increasing the lubricant viscosity generally provides better surface protection, resulting in lower wear. However, if the viscosity is too high, hydrodynamic lubrication will dominate and increase the drag force between the surfaces in motion. This is an important tradeoff to consider when designing a lubricant and must be considered and optimized for the application in question. Here there were quite a few lubricants that scored low in both friction coefficient and wear. The properties of these lubricants should be examined more closely to determine an optimal composition for a bicycle chain lubricant.

LUBRICANT STABILITY AND FUTURE WORK

5.1 Bio-derived Lubricant Stability

Natural oils are derived from a variety of common plants and exhibit exceptional lubrication performance, making them a highly desirable replacement for mineral or petroleum-based products, which are typically non-renewable, non-biodegradable, and can be toxic. One drawback to these oils, however, is their thermal and oxidative stability is generally much lower than that of their synthetic and petroleum-based counterparts. Vegetable oils typically have lower oxidative stability due to the presence of unsaturated sites (C-C double bonds) on the fatty acids chains of the triglycerides that make up 90-98% of these oils.⁸ Alkyl radicals can form at these sites and react with oxygen to form hydroperoxides and peroxides. These reactions degrade the oil by disrupting its structure over time, leading to a decline in lubrication performance.

Free radical formation and subsequent oxidation propagates the formation of new free radicals, creating a chain reaction known as autoxidation.⁸ Due to this effect, oils with a greater degree of unsaturation will undergo faster degradation than those that are mostly saturated. Therefore, vegetable oils with a high percentage of polyunsaturated fatty acids (e.g. linoleic and linolenic acid) will readily autoxidize at room temperature, whereas oils with a larger percentage of monounsaturated fatty acids will only autoxidize at high temperatures.⁸ Common oils high in polyunsaturated fatty acids include corn, cottonseed, and soybean oils.²⁷

There are many subsequent oxidation reactions that can occur after the initial hydroperoxide formation, leading to numerous intermediates and products that each

may have an effect on the performance of the lubricant. These secondary oxidation products are broken down into four categories: volatile, non-volatile, high molecular weight, and free fatty acid compounds.⁸ Fox and Stachowiak report in their article “Vegetable Oil-based Lubricants – A Review of Oxidation” that the presence of hydroperoxides in an oil decreases its wear rejection.⁸ It has been shown that the presence of free fatty acids actually improves boundary layer lubrication properties, although it is believed that accumulation of these free fatty acids further reduces the oxidative stability, resulting in a compounding negative effect on the wear rejection.⁸ Not all of these products are detrimental to the oil’s performance, however. The effects of non-volatile and high molecular weight oxidation products on lubrication performance are largely unknown, however various examples have shown these components can increase the viscosity and oxidative stability of the oil with little effect on its performance.⁸ Volatile oxidation products include short chain hydrocarbons and alcohols, which are unlikely to have any impact on the lubrication performance.

Studies have been done to compare the thermal and oxidative stability of various natural oils. When castor oil, cottonseed oil, almond oil, and passion oil were compared, it was found that castor oil had the best stability under an inert atmosphere and increasing temperature, while the other oils had poor results.⁷ In an oxidative environment, castor oil still had the best stability, with cottonseed oil performing slightly worse.⁷ The authors of this study also experimented with adding a small amount of an antioxidant additive (1 wt. % Lubrizol 7652A) to improve stability. It was found that the performance of castor oil was relatively constant, while the other oils showed significant improvement with the additive.⁷ The castor oil’s

outperformance of the other oils is likely due to its unique structure. Castor oil is comprised of 80-90% ricinoleic acid, which is a monounsaturated fatty acid, making its degree of unsaturation lower than the other oils.⁸ Ricinoleic acid also contains a hydroxy group on the 12th carbon, which could lead to the increased stability, although the true reason for this observation is unknown.

In conclusion, bio-derived oils tend to have excellent lubrication properties, but are less resistant to oxidation and thermal degradation than petroleum-based lubricants. Addition of antioxidants is one solution, but one idea being explored is to modify the oil composition, or choose one with a naturally occurring optimum composition for the application in question. An oil with limited unsaturated fatty acid content is desired as these chains can degrade spontaneously at low temperatures. Since monounsaturated fatty acids have greater stability than polyunsaturated fatty acids and remain a fluid over a larger range of temperatures than fully saturated fatty acids, oils rich in monounsaturated fatty acids are likely the best candidates to be used as lubricants.

5.2 Future Work

Throughout the course of this research, many ideas came up that we would have liked to investigate, but did not have time for before the completion of this thesis. First, all of the lubricants considered in this study have been oil based liquid lubricants. There are a number of solid waxes and greases that can be tested to determine their performance in the context of bicycle chain lubrication. Additionally, samples can be created from mixtures of biodegradable and synthetic lubricants to better understand performance tradeoffs.

All of these experiments were run under ideal laboratory conditions, however this is rarely the case when cycling out in the natural environment. Chains can become dirty and wet quickly after riding in the elements for even a short period of time. For this reason it would be interesting to test the effect of dirt, grime, and water on the performance of these lubricants. A decline in performance would be expected but how significant of a decrease? Will some lubricants handle these conditions better than others? These are questions we would like to explore in the future. Samples can be created and tested by mixing defined amounts of dirt or water with known lubricant standards.

The final goal of this research, to develop a superior bicycle chain lubricant, was also not reached within the scope of this report. With the foundation laid here, and continual investigation and analysis, this goal can likely be attained in the foreseeable future. I wish the best of luck to the students continuing on with this project in the future.

REFERENCES

1. Anderson, William. "Basics of Lubrication." *Society of Tribologists and Lubrication Engineers* (2008) Web. 5 May 2015.
2. Bowden, F. P., and D. Tabor. "The Friction and Lubrication of Solids." *Oxford University Press* (1950) Print.
3. Brown, Sheldon. "Chain Maintenance." 2015. Web. 5 May 2015. <<http://sheldonbrown.com/chains.html>>.
4. "Chain Replacement and Repair." 2015. Web. 5 May 2015. <<http://thebicyclechain.com/how-to/chain-replacement-and-repair-pg80.htm>>.
5. Coles, Jeffrey M., Debby P. Chang, and Stefan Zauscher. "Molecular Mechanisms of Aqueous Boundary Lubrication by Mucinous Glycoproteins." *Current Opinion in Colloid & Interface Science* 15.6 (2010): 406-16. Web. 5 May 2015.
6. "D-510 PISeca Capacitive Sensors." 2015. Web. 5 May 2015. <<http://www.physikinstrumente.com/product-detail-page/d-510-500400.html>>.
7. Dos Santos Politi, Jose R., Rodrigues de Matos, Pablo R., and Maria J. Sales. "Comparative Study of the Oxidative and Thermal Stability of the Oxidative and Thermal Stability of Vegetable Oils to be used as Lubricant Bases." *Journal of Thermal Analytical Calorimetry* 111.2 (2012): 1437-42. Web. 12 May 2015.
8. Fox, N. J., and G. W. Stachowiak. "Vegetable Oil-Based Lubricants - A Review of Oxidation." *Tribology International* 40 (2006): 1035-46. Web. 12 May 2015.
9. "Friction Module: Asperities." 2000. Web. 5 May 2015. <<http://www.nano-world.org/frictionmodule/content/0200makroreibung/0500asperities/?lang=en>>.
10. Hart, Marion. "Tribology Makes the World Go 'Round." 2011. 5 May 2015. <<https://www.asme.org/engineering-topics/articles/tribology/tribology-makes-the-world-go-round>>.
11. "The Importance of Drive Chain Lubrication." 2014. Web. 5 May 2015. <http://www.diesalbikes.com/tech/tech_briefs/tb090124/tech_brief_tb090124.htm>.

12. Kidd, M. D., R. E. Loch, and R. L. Reuben. "Experimental Examination of Bicycle Chain Forces." *Experimental Mechanics* 34.4 (1999): 278-83. Print.
13. Kleimann, Colonel. "Solid Film Lubrication: A Practical Guide." *Machinery Lubrication* 3 (2006) Web. 5 May 2015.
14. Kopeliovich, Dmitri. "Lubrication Regimes." *Substances and Technologies* (2015) Web. 5 May 2015.
15. Kopeliovich, Dmitri. "Mechanisms of Wear." *Substances and Technologies* (2015) Web. 5 May 2015.
16. Milosev, Ingrid, Rihard Trebse, and Simon Kovac. "Survivorship and Retrieval Analysis of Sikomet Metal-on-Metal Total Hip Replacements at a Mean of Seven Years." *The Journal of Bone and Joint Surgery* 88.6 (2006): 1173-82. Web. 5 May 2015.
17. O'Hagan, David. "Understanding Organofluorine Chemistry: An Introduction to the C-F Bond." *Chemical Society Review* 37 (2008): 308-19. Web. 5 May 2015.
18. Palaci, Ismael. "Atomic Force Microscopy Studies of Nanotribology and Nanomechanics." École Polytechnique Federale de Lausanne, 2007. Web. 5 May 2015.
19. Paschotta, Rudiger. "Interferometers." *RP Photonics Encyclopedia* (2015) Web. 5 May 2015.
20. Prignon, Yves. "Equipment: Pin-on-disc." 2006. Web. 5 May 2015. <<http://www.metaux.ulg.ac.be/metaux/index.php?page=pin-on-disc>>.
21. Rabinowicz, Ernest. *Friction and Wear of Materials*. 2nd ed. Wiley-Interscience, 2013. Print.
22. "RDP LVDT: How it Works." 2015. Web. <<http://www.rdpe.com/us/hiw-lvdt.htm>>.
23. Spicer, James B., and Christopher J. K. Richardson. "Effects of Frictional Loss of Bicycle Chain Drive Efficiency." *Journal of Mechanical Design* 123 (2001): 598-605. Print.

24. Stachowiak, Gwidon W., and Andrew W. Batchelor. *Engineering Tribology*. 3rd ed. Burlington, MA: Elsevier Butterworth-Heinemann, 2005. Web. 5 May 2015.
25. "Tribology." 2015. Web. <<http://www.merriam-webster.com/dictionary/tribology>>.
26. Wright, Jeremy. "Grease Basics." *Machinery Lubrication* 5 (2008) Web. 5 May 2015
27. Zambiasi, Rui Carlos, et al. "Fatty Acid Composition of Vegetable Oils and Fats." *Curitiba* 25.1 (2007): 111-20. Web. 12 May 2015.
28. Ziemer, James. "Basics of Wear." Society of Tribologists and Lubrication Engineers (2008) Web. 5 May 2015.

Appendix A

LUBRICANT INFORMATION

Table A.1: Commercial lubricant samples with respective abbreviations.

| Sample | Sample ID |
|--------|---|
| 1-A | SLICK Lube Lite 50 |
| 1-B | SLICK Lube Original 100 |
| 1-C | SLICK Lube Xtreme 200 |
| 1-D | Finish Line Wet |
| 1-E | Pedros Syn |
| 1-F | Tri Flow |
| 1-G | Dumonde Tech Lite |
| 1-Q | ProLink ProGold |
| 1-R | Mobil 15W/50 |
| 1-S | Spin Doctor Wet Lube |
| 2-B | Dumonde Original |
| 2-C | Dumonde BioGreen G10 |
| 2-F | 3-in-1 Multipurpose oil |
| S-2 | Polyalphaolefin (PAO2) low |
| S-3 | Polyalphaolefin (PAO40) high |
| S-6 | Exo-Lube POE 220 |
| 1-H | Pure Wet |
| 1-K | Velo Yelo Nasty Wet |
| 1-M | Muc Off Wet (blue) |
| 2-M | Green Oil |
| 2-N | Finish Line Pro Road - Ceramically Reinforced |
| 2-P | White Lightning Wet Ride |
| 2-R | Tri Flow Superior Soy Lube |
| 2-V | Boeshield T-9 |
| 2-W | Pedros Go |
| 2-X | Park Tool CL-1 |
| 2-Y | GT85 |
| 2-D | WD40 Wet |
| 3-N | Gnar Lube - Black Sapphire (2 oz) |

Table A.2: Natural oil samples with respective abbreviations.

| Sample | Sample ID |
|--------|-----------------|
| S-1 | Canola Oil |
| SA-1 | Castor Oil |
| SA-2 | Olive Oil |
| SA-3 | Rape Seed Oil |
| SA-4 | Cotton Seed Oil |
| SA-5 | Corn Oil |
| SA-6 | Sesame Seed Oil |
| SA-7 | Peanut Oil |
| SA-8 | Linseed Oil |
| SA-10 | Soybean Oil |

Appendix B

DETAILED TRIBOMETER BLUEPRINTS

B.1 Stage, Legs, and Spindle

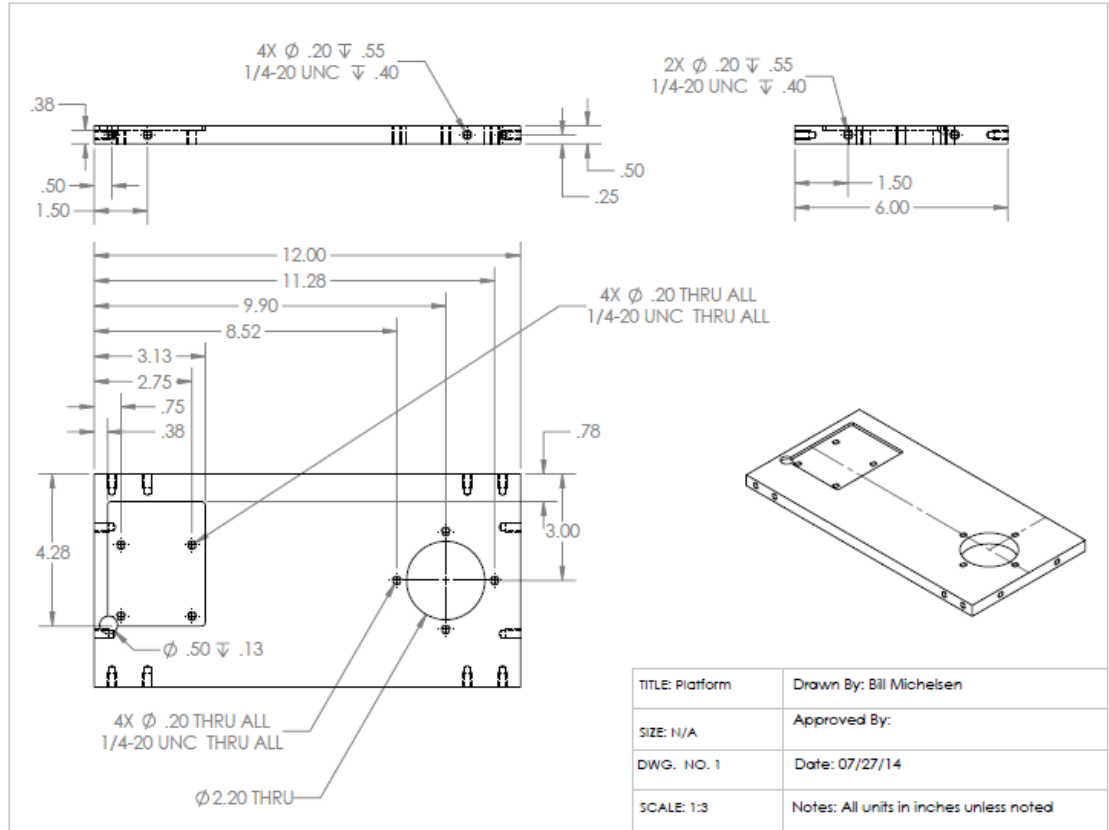


Figure B.1: Mounting stage specifications.

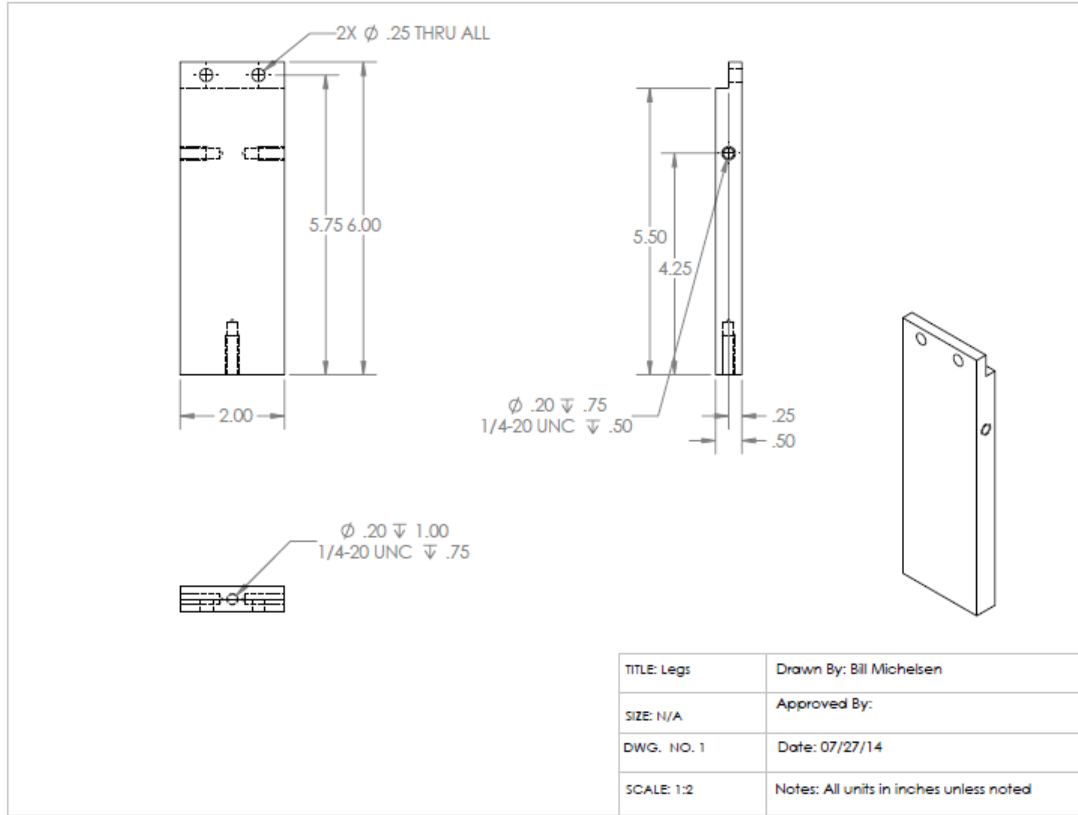


Figure B.2: Stage leg specifications. Four identical legs were machined.

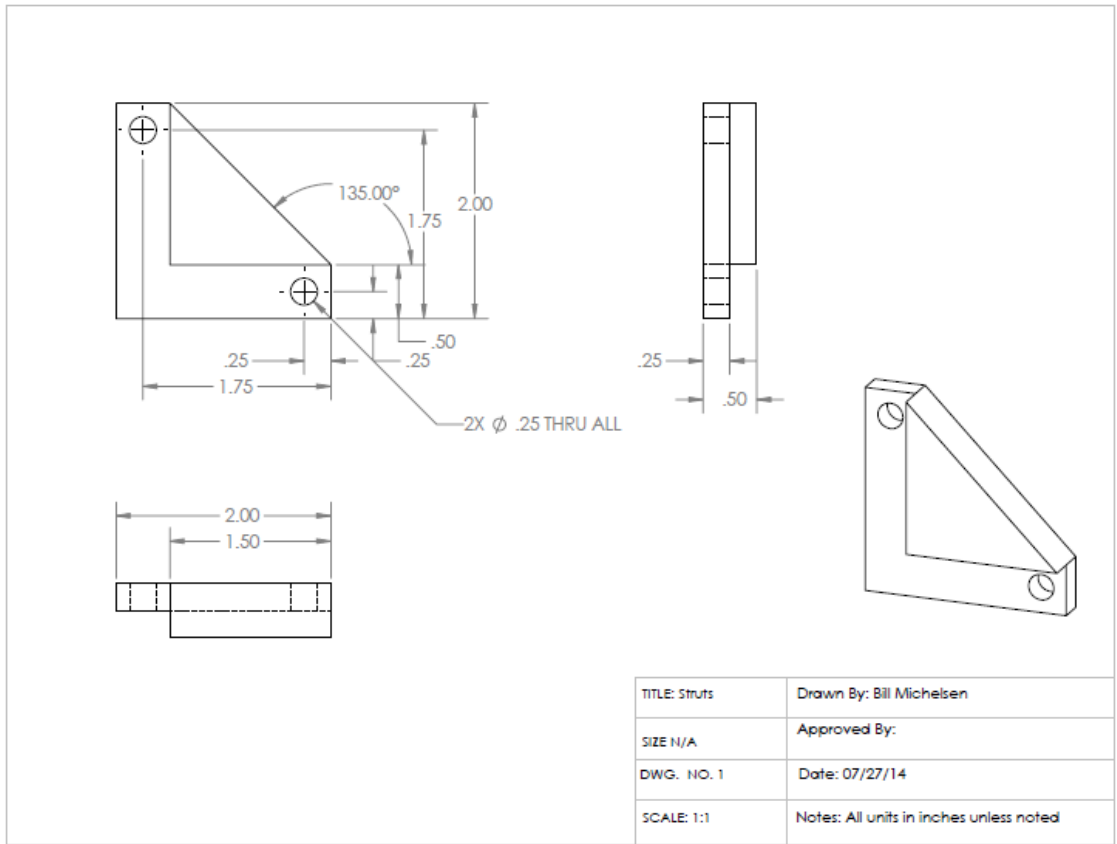


Figure B.3: Stage leg brackets. One attaches the side of each leg to the stage.

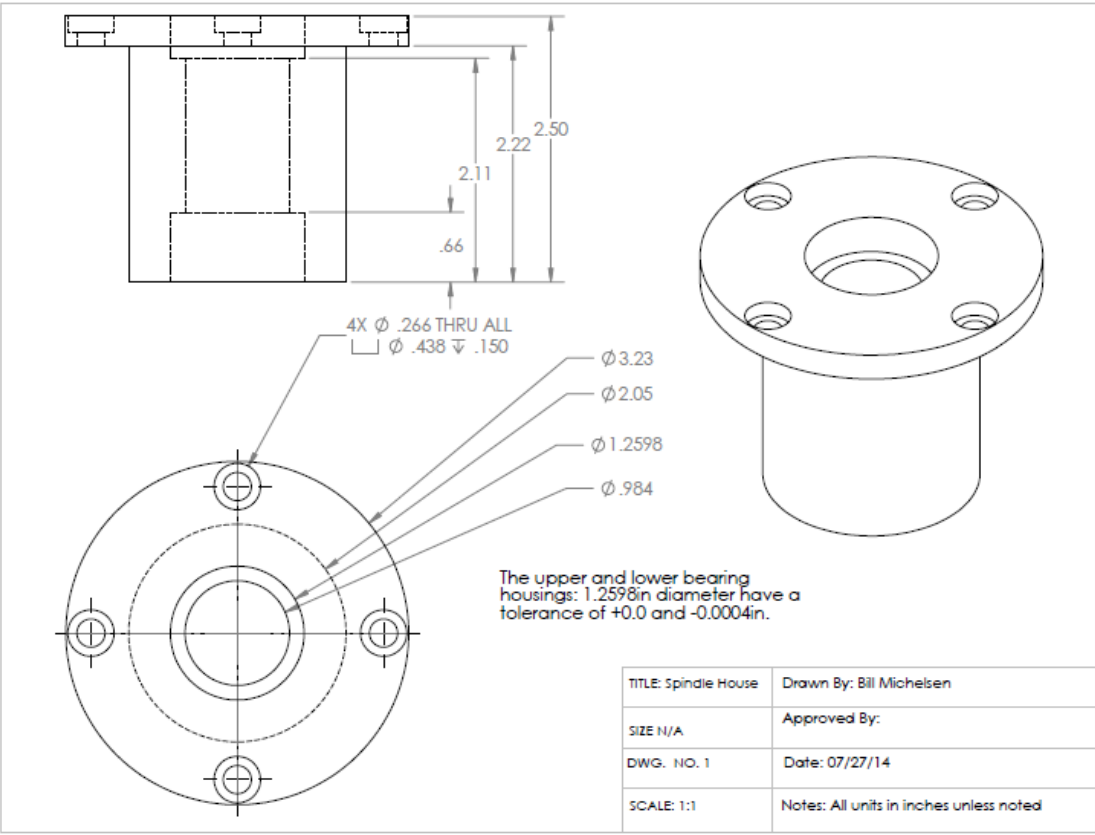


Figure B.4: Spindle housing. Angular contact bearings are fit into the wide spaces cleared at the top and bottom of the cylinder.

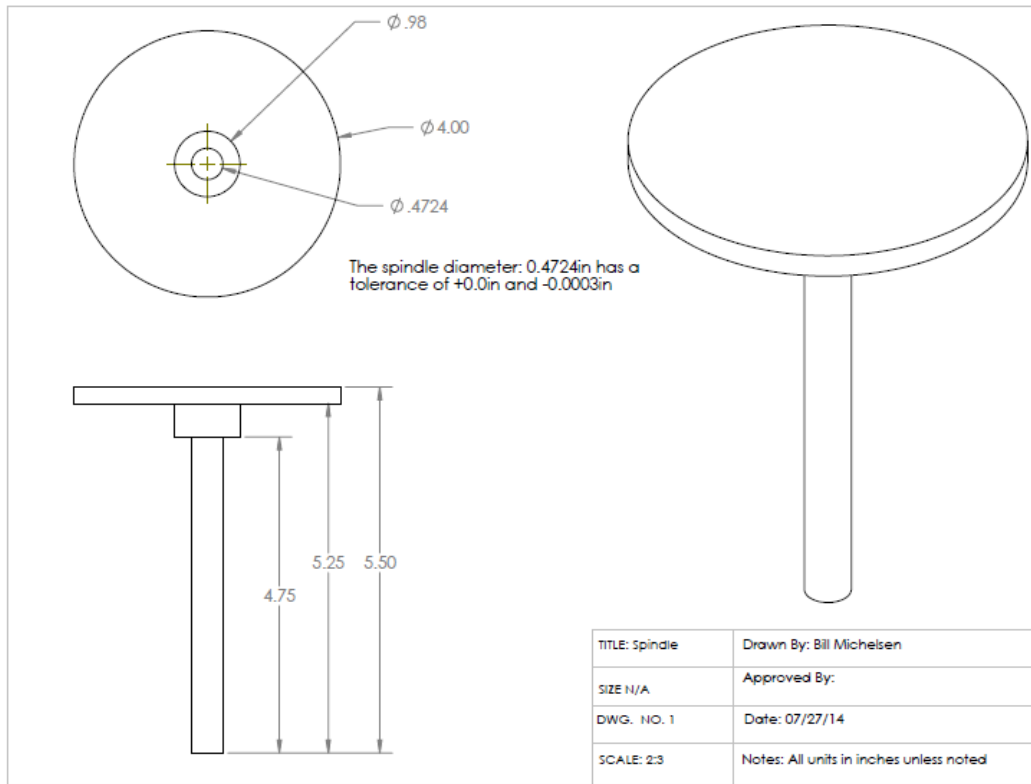


Figure B.5: Spindle and sample disc specifications, made from stainless steel.

B.2 Load Arm and Flexure Arms

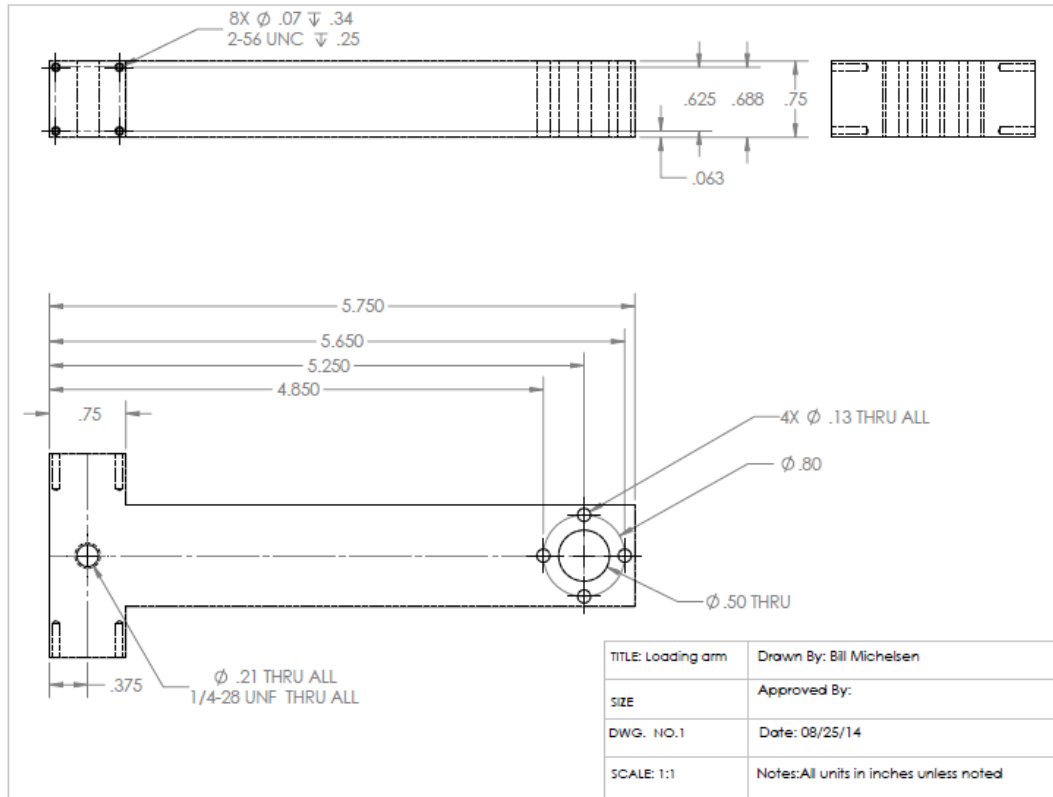


Figure B.6: Load arm specifications.

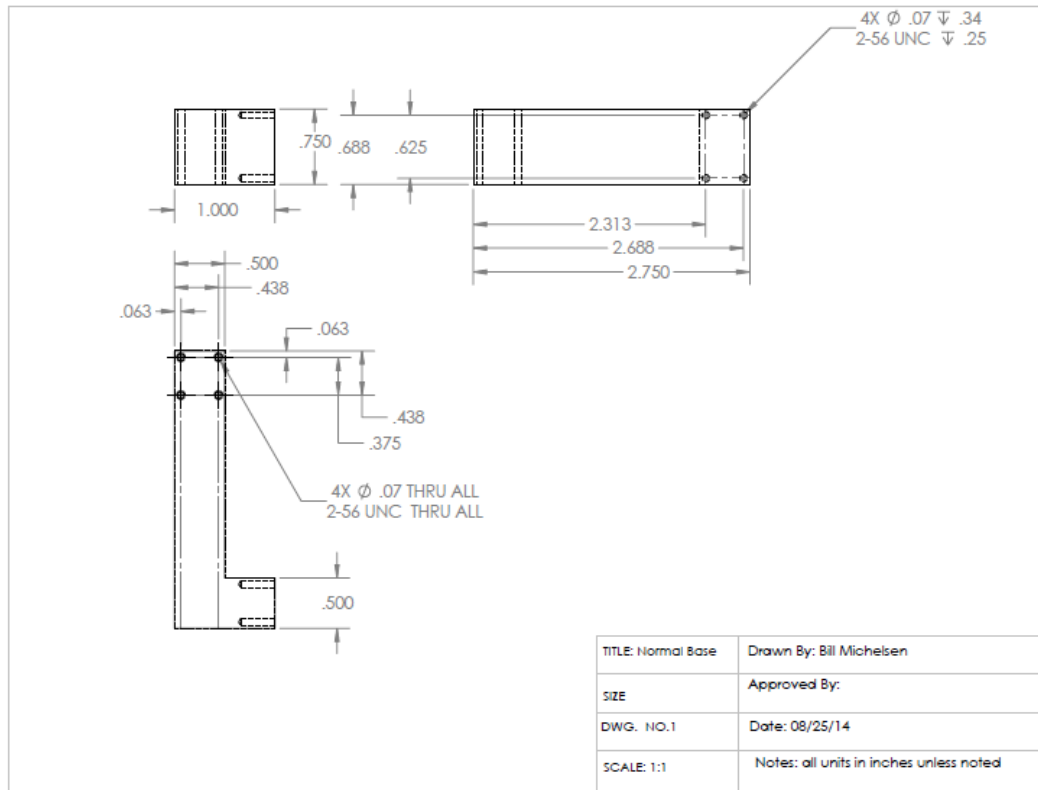


Figure B.7: Flexure arm specifications. Two identical arms are needed.

B.3 Back Mounting Plate and Spring Clamps

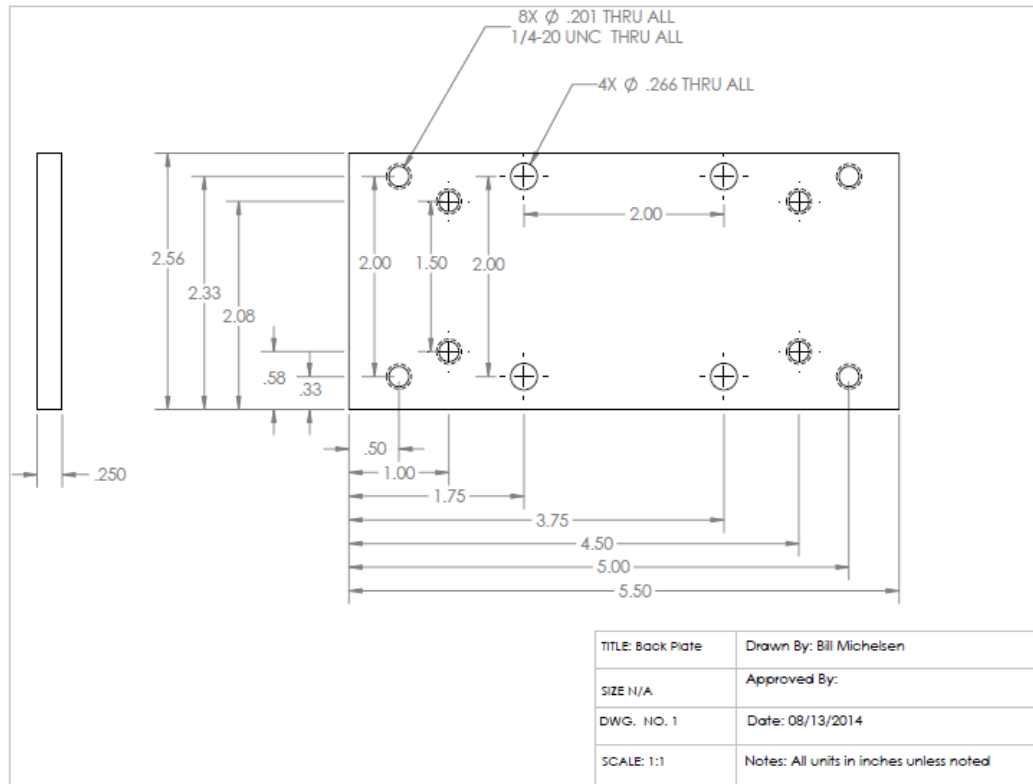


Figure B.8: Back plate. Includes holes for mounting to z-stage and for flexure arm and stopper arm attachments.

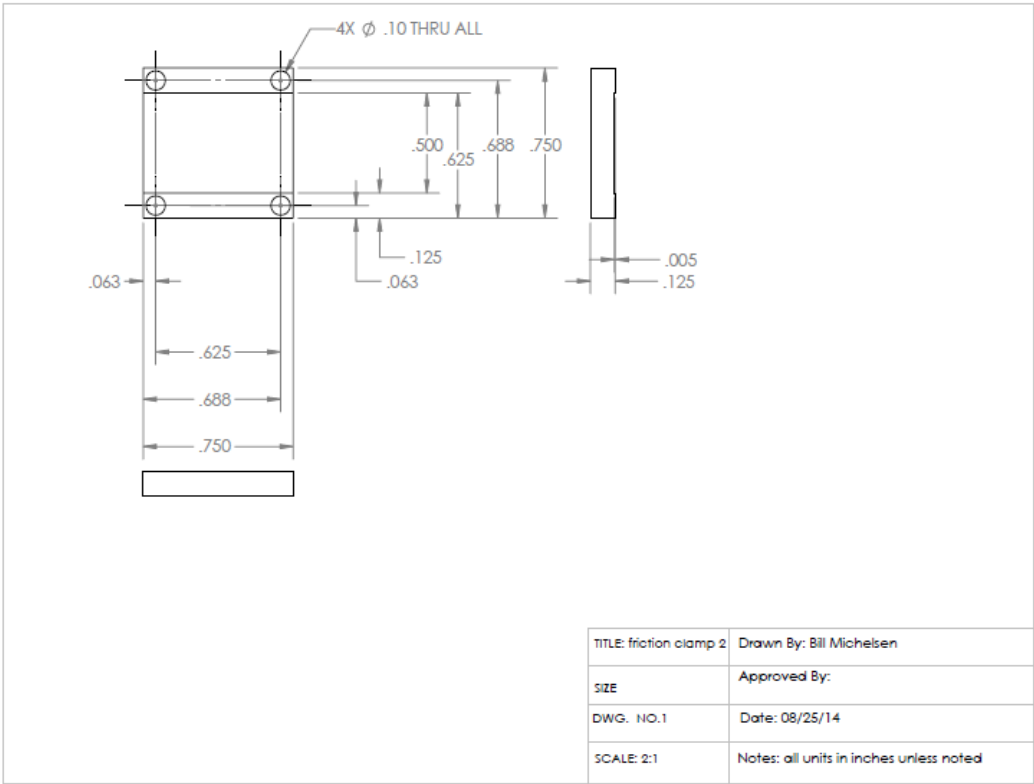


Figure B.9: Friction spring clamps. One of these attaches to each end of the load arm.

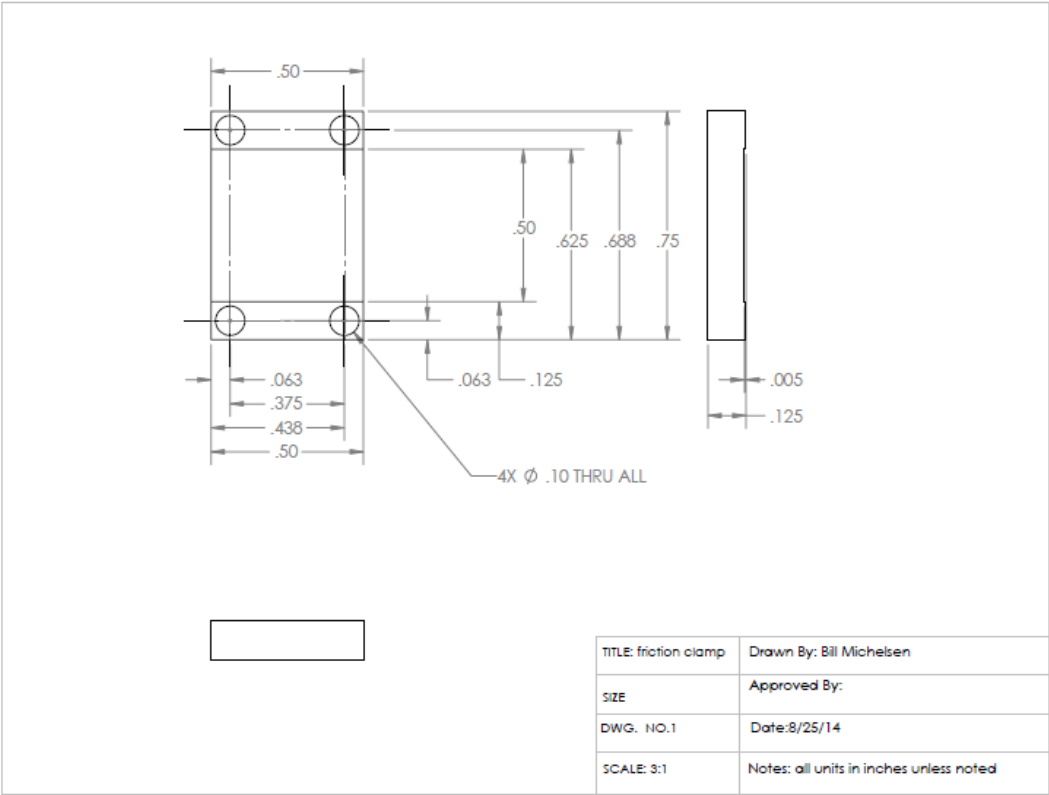


Figure B.10: Friction spring clamps. One of these attaches to each flexure arm end.

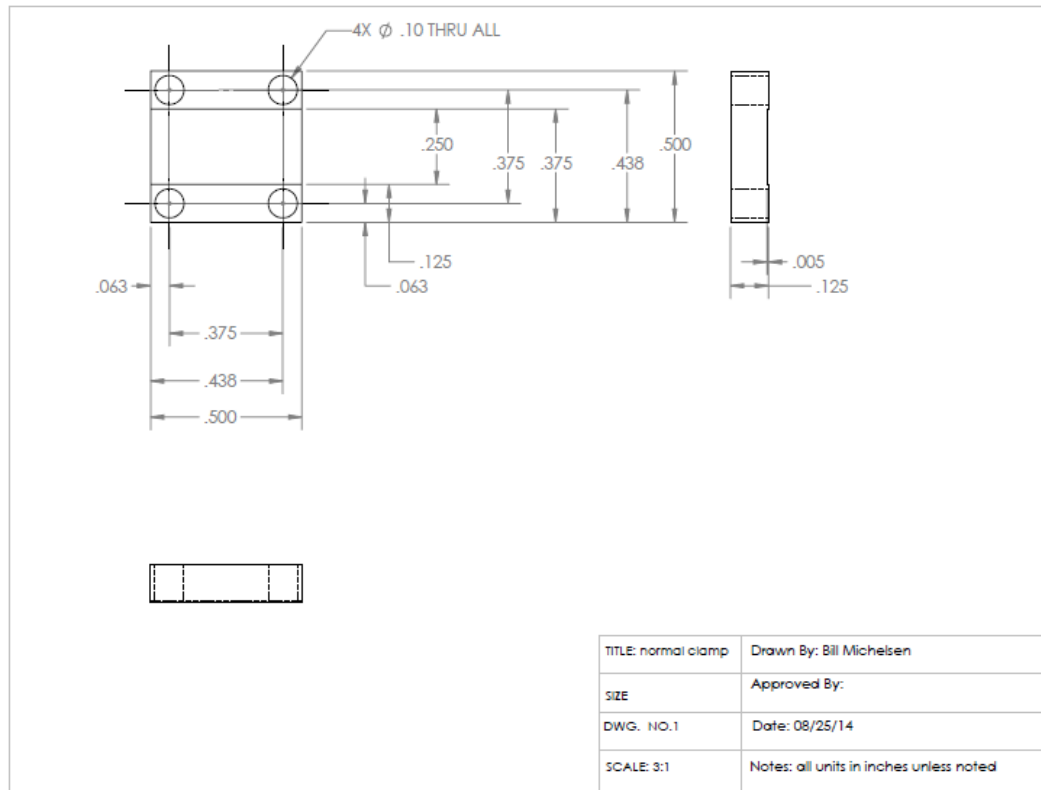


Figure B.11: Normal spring clamps. Four identical parts are needed: two for each flexure arm and two for each bracket attachment to the back plate.

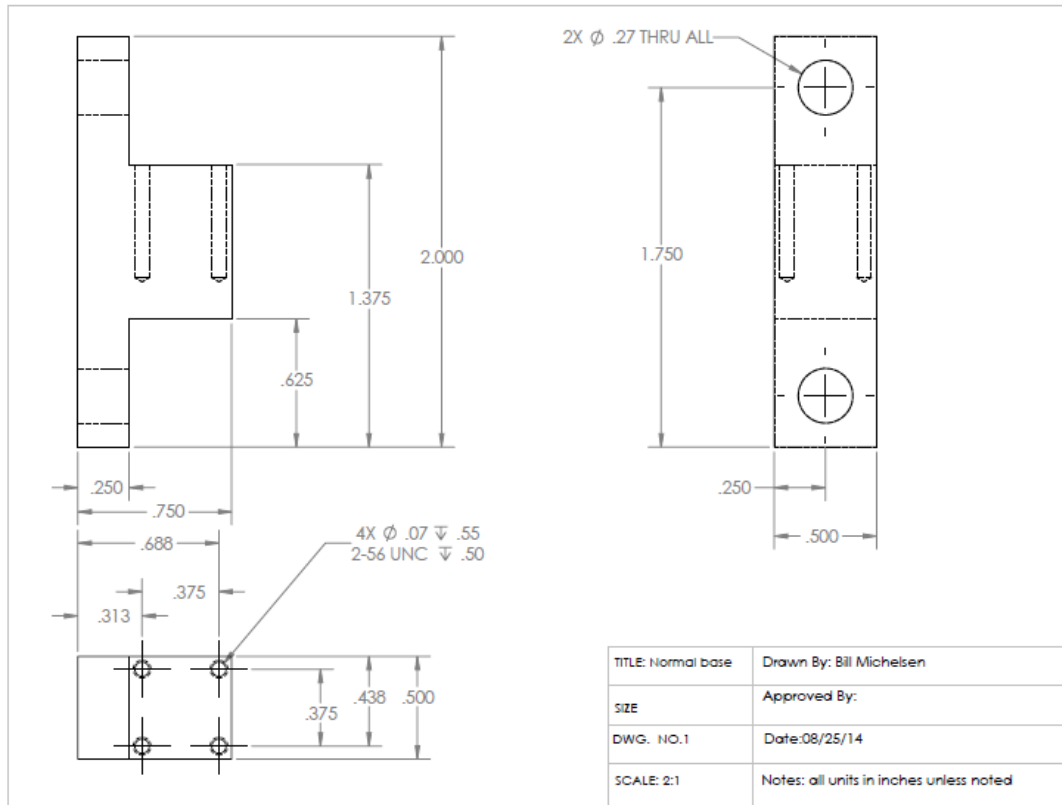


Figure B.12: Normal spring base brackets. These attach to the back plate and serve as the bases for the two normal force springs.

B.4 Stopper Arms and Ball Bearing Holder

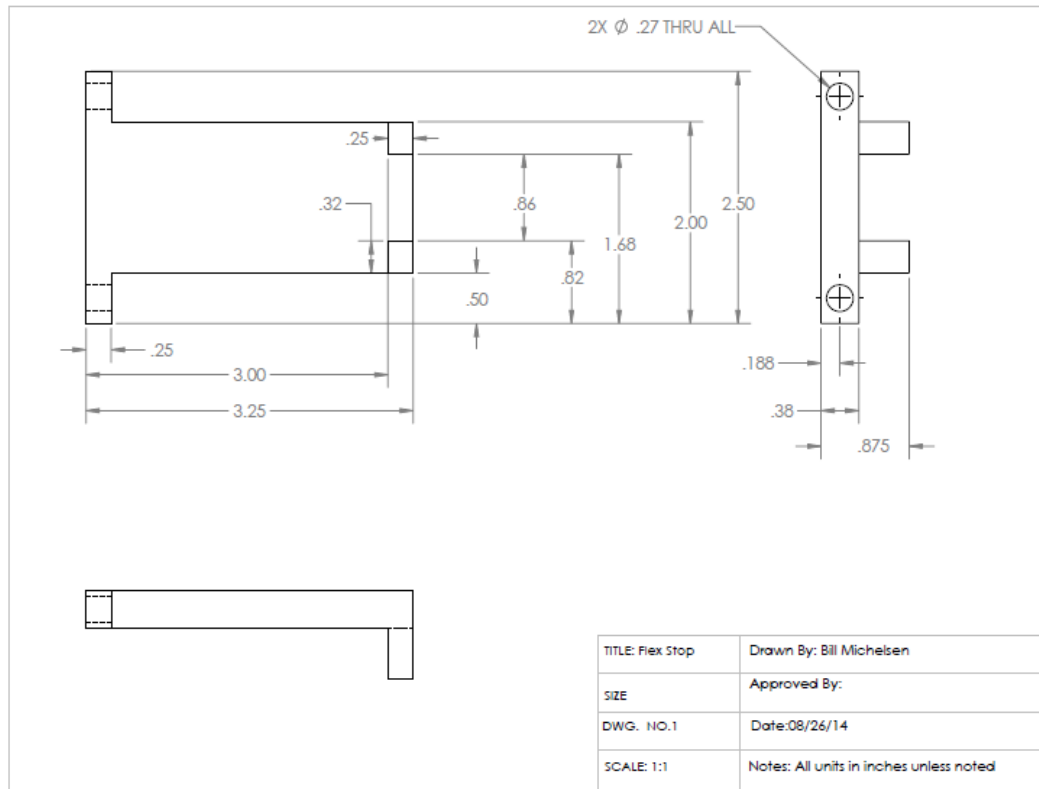


Figure B.13: Stopper arms to prevent over extension of normal force springs. One is needed for each flexure arm, however one side must have a section cut away to accommodate the friction sensor.

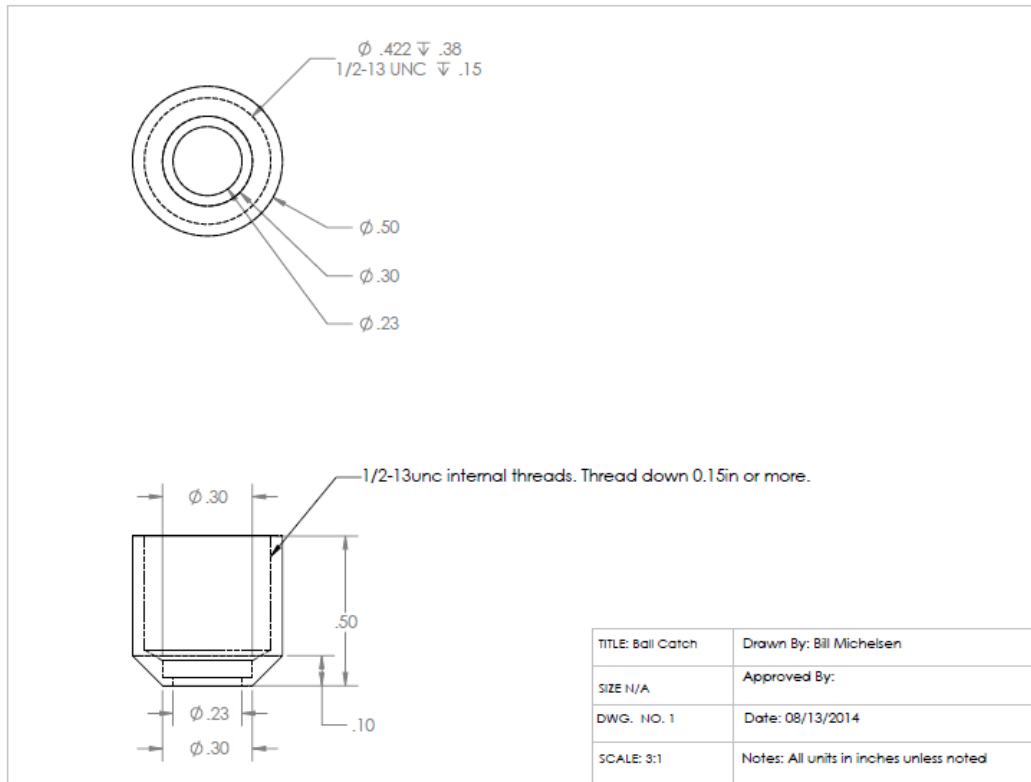


Figure B.14: Ball bearing holder. The inside is threaded for each removal to access to ball for cleaning or replacement.